NAVAL POSTGRADUATE SCHOOL
Monterey, California

THESIS

OPTIMIZING AEROBOT EXPLORATION OF VENUS

by

Kevin S. Ford

March, 1997

Thesis Advisor: Robert F. Dell

Approved for public release; distribution is unlimited

OPTIMIZING AEROBOT EXPLORATION OF VENUS

Kevin Sean Ford–Lieutenant, United States Navy
B.S. Physics, Florida State University, 1989

Venus Flyer Robot (VFR) is an aerobot—an autonomous balloon probe—designed for remote exploration of Earth's sister planet in 2003. VFR's simple navigation and control system permits travel to virtually any location on Venus, but it can survive for only a limited duration in the harsh Venusian environment. To help address this limitation, we develop: (1) a global circulation model that captures the most important characteristics of the Venusian atmosphere; (2) a simple aerobot model that captures thermal restrictions faced by VFR at Venus; and (3) one exact and two heuristic algorithms that, using abstractions (1) and (2), construct routes making the best use of VFR's limited lifetime. We demonstrate this modeling by planning several small example missions and a prototypical mission that explores numerous interesting sites recently documented in the planetary geology literature.

Master of Science in Operations Research, March, 1997

Advisor: Robert F. Dell, Department of Operations Research
Second Reader: James N. Eagle, Department of Operations Research

REPORT DOCUMENTATION PAGE

Form Approved OMB No. 0704-0188

1. AGENCY USE ONLY (*Leave blank*)	2. REPORT DATE	3. REPORT TYPE AND DATES COVERED
	March, 1997	Master's Thesis

4. TITLE AND SUBTITLE	5. FUNDING NUMBERS
OPTIMIZING AEROBOT EXPLORATION OF VENUS	

6. AUTHOR(S)
Ford, Kevin S.

7. PERFORMING ORGANIZATION NAME(S) AND ADDRESS(ES)	8. PERFORMING ORGANIZATION REPORT NUMBER
Naval Postgraduate School Monterey, CA 93943-5000	

9. SPONSORING/MONITORING AGENCY NAME(S) AND ADDRESS(ES)	10. SPONSORING/MONITORING AGENCY REPORT NUMBER
Jet Propulsion Laboratory 4800 Oak Grove Drive, Pasadena, CA 91109	

11. SUPPLEMENTARY NOTES
The views expressed in this thesis are those of the author and do not reflect the official policy or position of the Department of Defense or the U.S. Government

12a. DISTRIBUTION/AVAILABILITY STATEMENT	12b. DISTRIBUTION CODE
Approved for public release; distribution is unlimited	

13. ABSTRACT(*maximum 200 words*)

Venus Flyer Robot (VFR) is an aerobot—an autonomous balloon probe—designed for remote exploration of Earth's sister planet in 2003. VFR's simple navigation and control system permits travel to virtually any location on Venus, but it can survive for only a limited duration in the harsh Venusian environment. To help address this limitation, we develop: (1) a global circulation model that captures the most important characteristics of the Venusian atmosphere; (2) a simple aerobot model that captures thermal restrictions faced by VFR at Venus; and (3) one exact and two heuristic algorithms that, using abstractions (1) and (2), construct routes making the best use of VFR's limited lifetime. We demonstrate this modeling by planning several small example missions and a prototypical mission that explores numerous interesting sites recently documented in the planetary geology literature.

14. SUBJECT TERMS		15. NUMBER OF PAGES
Planetary Exploration, Balloon, Aerobot, Aerovehicle, Robotics, Orienteering, Optimization		90
		16. PRICE CODE

17. SECURITY CLASSIFICATION OF REPORT	18. SECURITY CLASSIFICATION OF THIS PAGE	19. SECURITY CLASSIFICATION OF ABSTRACT	20. LIMITATION OF ABSTRACT
Unclassified	Unclassified	Unclassified	UL

NSN 7540-01-280-5500

Standard Form 298 (Rev. 2-89)
Prescribed by ANSI Std. 239-18 298-102

OPTIMIZING AEROBOT EXPLORATION OF VENUS

Kevin S. Ford
Lieutenant, United States Navy
B.S. Physics, Florida State University, 1989

Submitted in partial fulfillment of the
requirements for the degree of

MASTER OF SCIENCE IN OPERATIONS RESEARCH

from the

NAVAL POSTGRADUATE SCHOOL
March, 1997

Author: _____

Kevin S. Ford

Approved by: _____

Robert F. Dell, Thesis Advisor

_____

James N. Eagle, Second Reader

_____

Frank Petho, Chairman
Department of Operations Research

iv

ABSTRACT

Venus Flyer Robot (VFR) is an aerobot—an autonomous balloon probe—designed for remote exploration of Earth's sister planet in 2003. VFR's simple navigation and control system permits travel to virtually any location on Venus, but it can survive for only a limited duration in the harsh Venusian environment. To help address this limitation, we develop: (1) a global circulation model that captures the most important characteristics of the Venusian atmosphere; (2) a simple aerobot model that captures thermal restrictions faced by VFR at Venus; and (3) one exact and two heuristic algorithms that, using abstractions (1) and (2), construct routes making the best use of VFR's limited lifetime. We demonstrate this modeling by planning several small example missions and a prototypical mission that explores numerous interesting sites recently documented in the planetary geology literature.

THESIS DISCLAIMER

The reader is cautioned that computer programs developed in this research may not have been exercised for all cases of interest. Although every effort has been made to ensure that the programs are free of computational and logic errors, they cannot be considered as having been validated. Any application of these programs without additional verification is at the risk of the user.

TABLE OF CONTENTS

LIST OF FIGURES

LIST OF TABLES

ACKNOWLEDGMENT

EXECUTIVE SUMMARY

The NASA Jet Propulsion Laboratory (JPL) performs the vast majority of planetary exploration done by the United States (US) and represents the US in most multinational missions. JPL uses robotic vehicles to explore other worlds and they are now in the early stages of developing a three-dimensional roving robot called an aerobot—an *aero*vehicle for ro*botic* exploration. An aerobot is an exploration probe supported against a planet's gravity by the buoyancy of a balloon. For horizontal movement, it drifts on the wind. This recent innovation holds tremendous promise for helping scientists learn about any planet with an atmosphere, and there are many of these in our solar system. However, with the added capability that an aerobot brings to planetary exploration we find a whole new realm of questions regarding how best to use it. For example, an aerobot can probably reach any site on a planet. This sort of mobility is completely without precedent for an exploration robot, so the question of what route to use in going from one spot to another has never been too important—they've never been very far apart. With an aerobot, however, it is a crucial question. One route to a destination might take it near many other interesting places enroute. Because of this large exploration domain, there are more interesting sites on any world than a single aerobot has time to visit. This implies that the amount of interesting data an aerobot collects can differ radically depending upon its travel routes. Therefore, it is important that scientists prioritize these interesting sites and explore them in a rational, methodical way so as to make the best use of an aerobot's exploration time.

Venus Flyer Robot (VFR) is an aerobot designed for remote exploration of Earth's sister planet in 2003. VFR's simple navigation and control system permits travel to virtually any location on Venus, but it can survive for only a limited duration in the harsh Venusian environment. This thesis helps address this limitation: We develop a Global Circulation Model (GCM) of the Venusian atmosphere that captures position, distance, wind velocity, travel time (based on wind velocity), temperature, and other important characteristics in a graph—a set of nodes with arcs connecting these nodes. We also develop a simple aerobot model that captures thermal restrictions faced by VFR at Venus. Using these two abstractions and three path planning algorithms (one exact, and two heuristic) we also develop, we construct routes that make the best use of VFR's limited exploration time.

We demonstrate the utility of these tools by using all three algorithms to plan routes for several small example missions and use the two heuristics to plan routes for a much more realistic mission that explores numerous interesting sites recently documented in the

planetary geology literature. Besides determining a good route for exploration of several different sites, the planning aids we develop are useful in answering a number of other important questions. For example, we can use them to quantitatively study the importance of an aerobot's design lifetime, to explore the value of beginning exploration at different atmosphere insertion points, and to study the cost-effectiveness of different aerobot designs.

I. BACKGROUND

A. INTRODUCTION

Venus Flyer Robot (VFR) is an aerobot—an autonomous balloon probe—designed for remote exploration of Earth's sister planet in 2003. VFR's simple navigation and control system permits travel to virtually any location on Venus, but it can survive for only a limited duration in the harsh Venusian environment. To help address this limitation, this thesis (1) develops a graph implementation of a global circulation model that captures position, distance, wind velocity, travel-time (based on wind velocity), temperature, and other characteristics of the Venusian atmosphere. (2) implements a simple aerobot model that captures thermal restrictions faced by VFR at Venus, and (3) presents one exact and two heuristic algorithms that use these two abstractions to construct routes making the best use of VFR's limited lifetime on Venus.

B. PLANETARY EXPLORATION USING ROBOTS

The NASA Jet Propulsion Laboratory (JPL) performs the vast majority of planetary exploration done by the United States (US) and represents the US in most multinational missions. JPL uses robotic vehicles to explore other worlds. These robots have evolved considerably over time.

Fly-by probes travel to an object of interest with great speed and never slow down. Their high velocity is both good and bad. It offers very short travel times, but it also limits the time a probe spends in close proximity to a target, resulting in little time for data collection. Some past fly-by robots and their prime targets were: Mariner 2 to Venus; Mariner 4 to Mars; and Voyagers 1 and 2 which explored the outer planets. Fly-by probes are simple, cheap, and ideal for the first visit to a planet. For example, JPL's Pluto Express mission consists of two fly-by probes to be launched in 2001. These probes will journey through space for about ten years before arriving at Pluto and its moon, Charon.

An orbiting probe, as the name implies, provides an extended period of time while orbiting a planet for data collection. Examples of orbiting robots are the Mariner 9 probe at Mars, the Magellan probe that collected radar imagery on about 98% of the Venusian surface (Figure 1.1), and the Galileo orbiter—currently studying Jupiter and its 16 moons.

Another slightly more advanced robot is a lander. It spends a long time performing extensive studies on the surface of its target planet. Two examples are Vikings 1 and 2 which landed on Mars in the 1970's. Viking 1 touched down in a moderately cratered,

low-lying volcanic plain called Chryse Planitia. This is an old drainage region of a large outflow channel that almost certainly contained liquid water in the past. Viking 2 landed 6,460 km (4,014 miles) away in Utopia Planitia, a rock-strewn desert. Over the course of several Martian seasons, each of these robots collected detailed information about Martian weather, geology, and even conducted experiments to test for the presence of microbial life in the soil.

The next generation of robots for planetary research is a family of remotely controlled or autonomous rovers. Although not robotic, the first extraterrestrial rover was demonstrated on Earth's moon during the Apollo 15 mission in July 1971. Despite the fact that it was human-controlled, it did possess the most useful feature of roving devices— mobility. This feature, decoupled from the necessity of an on-board human operator, is extremely attractive for remotely exploring any hostile environment.

The main feature of JPL's Mars Pathfinder mission, launched in December 1996, is Sojourner—the first roving robot to visit another planet. Sojourner is a small, six-wheeled, partially autonomous, surface roving machine that can travel tens of meters from its home base. It represents the cutting edge in robotic development for vehicles navigating in two physical dimensions [Eisen 1996].

Although robot navigation in three physical dimensions is more difficult, it offers more capability than its two-dimensional counterpart. Assuming Sojourner can travel roughly 50 m from its home base, it has access to a circular region with area, $A = \pi r^2$, or, $7,854\,\mathrm{m}^2$. By contrast, a three-dimensional rover has access to the entire surface of its target world. In the case of Venus (mean planetary radius of 6,052 km), this is approximately $4.6 \times 10^{14}\,\mathrm{m}^2$. Hence, there is a vastly greater physical domain available to a three-dimensional robot—this is firm motivation for tackling the additional difficulty in implementing such a device.

JPL is now in the early stages of developing a three-dimensional roving robot called an aerobot—an *aero*vehicle for ro*bot*ic exploration. A planetary aerobot is an exploration probe supported against a planet's gravity by the buoyancy of a balloon [Cutts *et al.* 1995]. Figure 1.2 shows a schematic of an aerobot exploring Venus.

An aerobot is truly an innovative device in that the basic physics permitting its operation have been well understood for more than 50 years, but these principles have been applied in a new way with the development of balloons for remote planetary exploration.

C. THE PLANETARY AEROBOT

Although their enhanced mobility is the greatest advantage aerobots offer over previous generations of robotic vehicles, they have another, perhaps equally valuable advantage—they consume miniscule quantities of energy in accomplishing this mobility. Various methods of buoyancy control have been proposed for aerobots to best handle conditions at their various destinations. Currently, eight planets and moons are thought to have atmospheres sufficient to support an aerobot: Venus, Earth, Mars, Jupiter, Saturn, Titan (Saturn's largest moon), Uranus, and Neptune.

1. Altitude Control using Reversible Fluids

Although others are available, the most suitable method for aerobot altitude control at Venus uses reversible fluids [Jones 1995]. Most solutions to the general problem of controlling a balloon's altitude require the expenditure of large amounts of energy and/or matter. For example, in hydrogen or helium-filled balloons, the buoyancy gas has a smaller molecular mass than the surrounding air. This causes them to rise until atmospheric pressure is so small that differential pressure across the balloon material may cause it to rupture. Because of this unstable behavior, these balloons must frequently add or dump buoyancy gas to stay within some altitude band. However, a reversible fluid balloon solves the problem without these costly measures, making it an ideal device for remote exploration.

a. Passive Altitude Control

One method of aerobot altitude control that avoids the difficulty faced by helium balloons uses multiple gas balloons supporting one gondola. There is a primary balloon that contains a lighter-than-air gas such as helium, and at least one additional balloon containing a reversible fluid. In general, a *fluid* is either a gas or a liquid. A *reversible* fluid readily changes back and forth between these two states with changing temperature and pressure. The primary balloon supports the majority of the aerobot's mass, but not all of it—the aerobot sinks without the additional lift provided by the other balloon(s).

The major advantage of this method is that, left undisturbed, a properly configured reversible fluid aerobot oscillates about an equilibrium altitude (EA) where ambient conditions correspond to the saturation temperature and pressure of the reversible fluid. This oscillation occurs so long as atmospheric temperature decreases with increasing altitude in the vicinity of the EA. This often occurs in the troposphere, and while within

3

such a negative temperature gradient, an aerobot's altitude is passively controlled by a naturally occurring negative feedback cycle.

To understand this negative feedback cycle, consider one period in the cycle. When an aerobot is beneath its EA where ambient temperature is higher than saturation (boiling) temperature for that pressure, some fluid evaporates, increasing total balloon volume. This lowers the overall density (mass per volume) of the aerobot, causing it to rise. When it rises above its EA, the ambient temperature is lower than the saturation temperature and some of the fluid condenses back to its liquid state. This results in a lower overall volume for the aerobot, thus higher density, and the aerobot sinks. When it is again below its EA, the cycle recurs. JPL's Balloon Experiment at Venus (BEV), scheduled for 1999, will be capable of this passive altitude control, but nothing more. It is planned to oscillate between 40 and 60 km above the mean planetary radius [DiCicco *et al.* 1995].

b. Inexpensive Active Altitude Control

With naturally occurring characteristics of a target planet operating to passively maintain an aerobot's altitude in the manner described above, actively controlling altitude between its EA and the planetary surface becomes an extremely simple task.

By connecting a fixed-volume pressure vessel to the balloon into which the reversible fluid can drain, and permitting this pressure vessel to be isolated by means of a simple valve, it is possible to prevent the aerobot from regaining the extra buoyancy required to re-ascend after dropping below its EA. This is done by simply shutting its isolation valve. The sequence of events giving rise to this behavior is roughly as follows:

1. While positively buoyant, as the aerobot rises above its EA, the lower temperature there causes condensation of some fluid.

2. This fluid drains into the pressure vessel and the condensation continues to occur until the aerobot is again below its EA.

3. Once the aerobot is negatively buoyant and at any time while this remains the case, shutting the isolation valve between balloon and pressure vessel results in the aerobot remaining negatively buoyant, even long after it has sunk below EA.

It is impossible for the aerobot to become positively buoyant again as long as a certain percentage of the reversible fluid remains trapped within the fixed-volume pressure vessel since this portion can no longer change the volume of the reversible fluid balloon. In this state, the aerobot continues to sink until it comes into contact with the planetary surface. Thus, the aerobot can land at will.

Although crude, this method of active altitude control is extremely cheap on energy usage, and with the exception of helium diffusion through the primary balloon material, the fluid cycles described are all closed, so no matter needs replenishment. The result is a long lasting three-dimensional roving exploration probe with a very slight demand for energy—an ideal robot for planetary exploration.

c. Horizontal Mobility

With active altitude control as an innate characteristic of an aerobot, the issue of controlling its position in the other two physical dimensions depends only upon the availability of horizontal forces to move the robot. This portion of an aerobot's control is also supplied by the target planet in the form of global winds.

Any planet in possession of an atmosphere has naturally occurring winds that arise from influences like insolation (solar heating), planetary rotation, and tidal forces. To navigate from one surface site to another, an aerobot need only drift on different winds at different altitudes until it reaches its destination. After collecting whatever data is available there, it can rise again (by opening its isolation valve) and move on to the next destination.

Thus, with buoyancy and altitude control comes a very simple but effective means of navigational control. So equipped, an aerobot is mobile in all three dimensions and possesses some measure of active control over its journey. The design of Venus Flyer Robot (VFR) includes all of these capabilities [Cutts *et al.* 1995]. We show an artist's conception of VFR at one of many sites on Venus in Figure 1.3.

d. Where to Explore First

Venus has already been identified as the first target planet for aerobot exploration. VFR's goal launch date is sometime in the year 2003 following a passive altitude control demonstration—the BEV mission planned for 1999. Two exploration balloons, the Vega probes, have already flown at Venus as part of a multinational collaboration between Russian, French, and US scientists [Blamont *et al.* 1986, Kremnev *et al.* 1986, Linkin *et al.* 1986a, Linkin *et al.* 1986b, Preston *et al.* 1986, Sagdeev *et al.* 1986a, Sagdeev *et al.* 1986b]. They were deployed in 1985 by two spacecraft on their way to a rendezvous with Halley's Comet. Venus is an ideal first target for many reasons:

1. The atmosphere of Venus is very hot, dense, and contains high concentrations of extremely corrosive chemicals such as sulfuric acid. The environment becomes more hazardous with proximity to the planet's surface, so the aerobot's altitude

control makes it an ideal choice for exploring Venus. It can dip into the harsh depths of the atmosphere for short periods of data collection and then rise out of harm's way back to cooler, more pleasant environs at cloud-top.

2. There are gale force winds blowing on Venus which offer good horizontal mobility for an aerobot. These winds are fairly predictable, so path planning is possible.

3. Although somewhat predictable, the Venusian atmosphere is still the subject of intense scientific debate because physical driving processes responsible for the global wind patterns have yet to be satisfactorily explained—much more atmospheric data is still required for this question to be adequately addressed. An aerobot is thus an ideal exploratory device because it collects atmospheric data enroute to various surface locations, effectively performing double-duty in data collection.

4. Many exploration probes such as Pioneer Venus Orbiter and Magellan have been sent to Venus. Based on information from these probes, scientists know a great deal about the surface of Venus. As mentioned earlier, Magellan collected a nearly complete global radar map of the Venusian surface (Figure 1.1). This information allows extensive planning regarding what surface locations warrant further study by an aerobot. Head *et al.* [1996] discuss several of these locations.

5. Venus is only a short jaunt for an Earth-launched space probe, so travel time is short—the BEV expected travel time from Earth to Venus is only four months. Therefore, lessons learned from BEV can be quickly incorporated into VFR.

D. OPTIMAL EXPLORATION

Although capable of navigating to virtually any location on the surface of a planet (limited only by global wind patterns), an aerobot is still constrained by its lifetime. Exposure to hostile elements can adversely effect the robot, leading eventually to its demise. There simply are many more sites on any world that might be explored than a single aerobot will have time to visit. Therefore, it is important that scientists prioritize these sites and explore them in a rational, methodical way so as to return the largest quantity of the most valuable data possible (scientific value). This thesis brings just such a rational, methodical approach to planetary exploration using aerobots. Specifically, it presents several three-dimensional path planning algorithms that find routes with the largest scientific value obtainable in an aerobot's lifetime.

In the following pages, Chapter II discusses recent path planning research and how it relates to the problem posed in this thesis. Chapter III states the problem and Chapter IV

describes the algorithms developed for solving it. Finally, Chapter V presents the results of several example problems, highlighting the effectiveness of these algorithms, and Chapter VI provides conclusions and recommendations for further research.
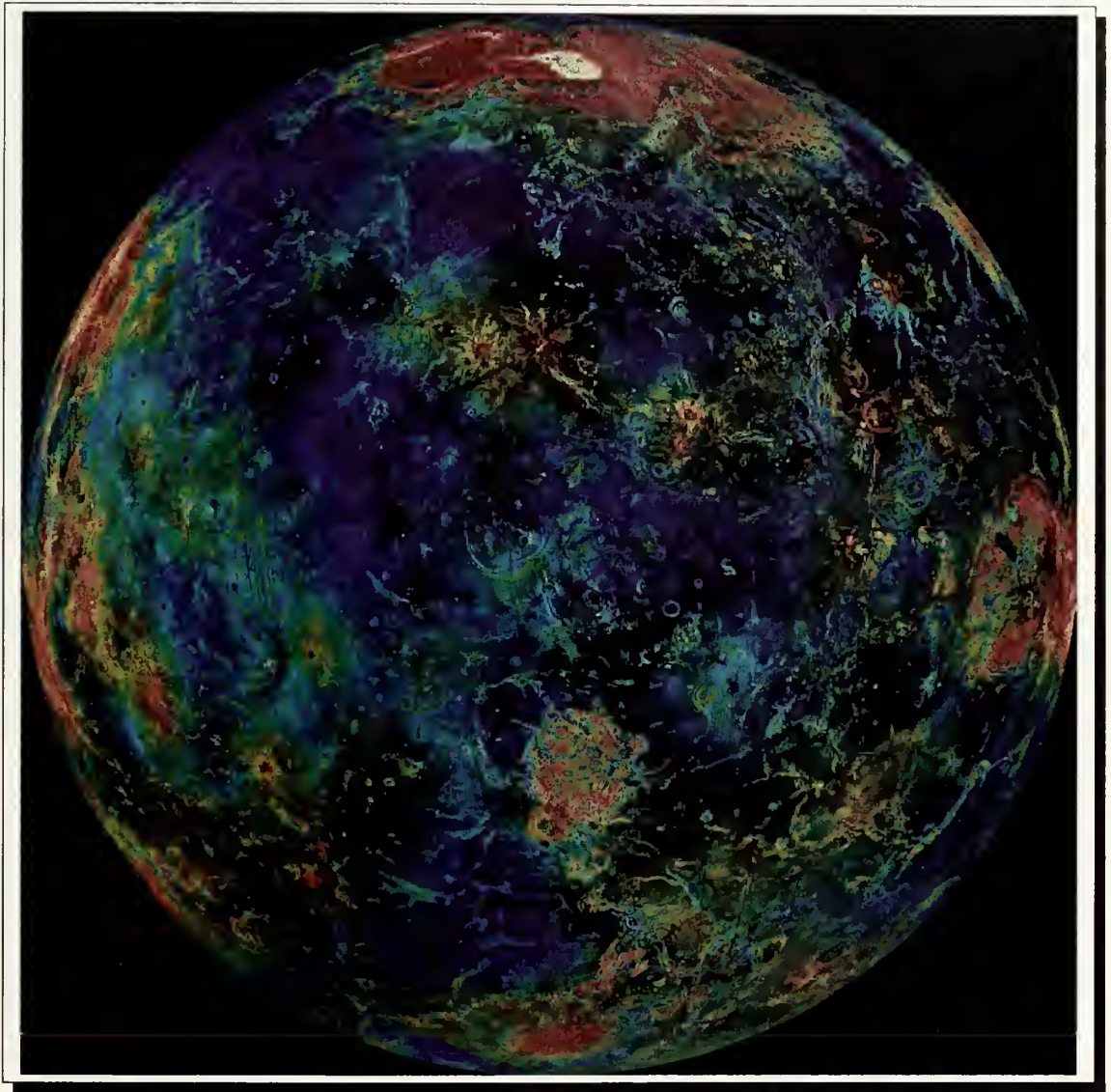
Figure 1.1. An orthographic projection of Venus (centered at 0°E longitude), simulating a distant view of one hemisphere of the planet. This image represents more than a decade of radar investigation culminating in the 1990–1994 Magellan mission. Magellan imaged more than 98 percent of Venus at a resolution of ~100 m; the effective resolution of this image is ~3 km. A mosaic of Magellan images (most with illumination from the west) forms the image base. Data from the Arecibo radio telescope in Puerto Rico and the Russian Venera and US Pioneer Venus missions fill gaps in Magellan's coverage. The Jet Propulsion Laboratory (JPL) in Pasadena, CA managed the Magellan mission for NASA. (Courtesy NASA/JPL) Source: http://bang.lanl.gov/solarsys/venus.htm.
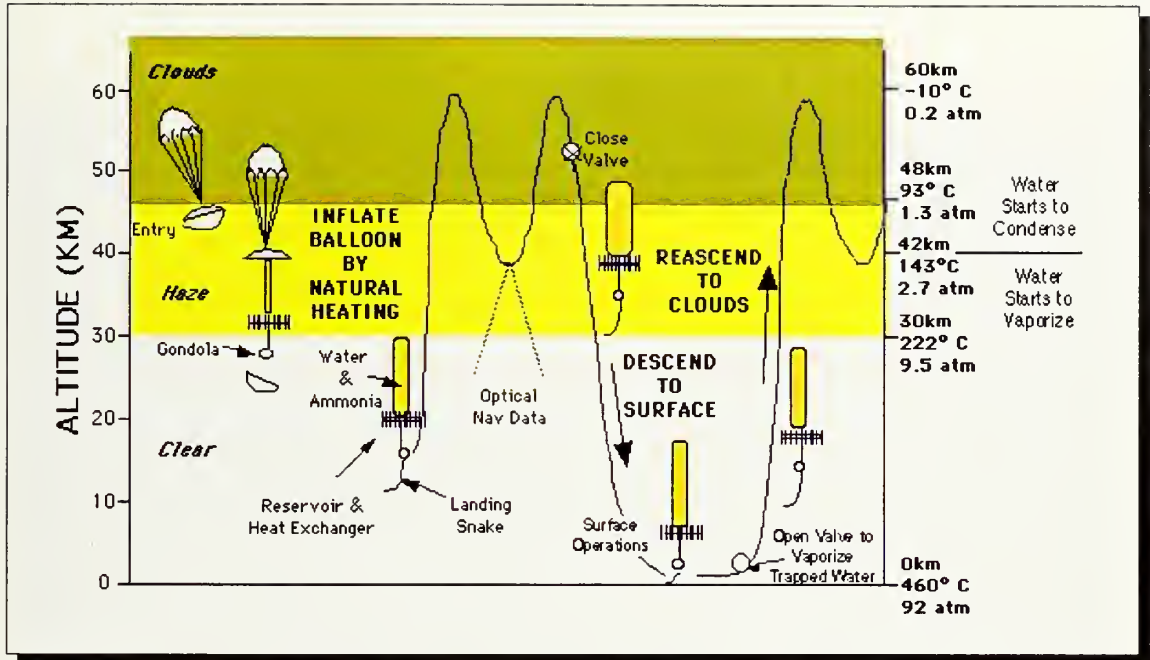
Figure 1.2. A planetary aerobot performing several steps in a typical mission to explore the planet Venus. Starting on the far left and progressing chronologically to the right, the probe first enters the Venusian atmosphere, deploys various aerobraking techniques to slow down from orbital velocity, and jettisons the heat shield. Its balloons then inflate through natural heating by the surrounding atmosphere, and the probe begins oscillating about its equilibrium altitude. During the lower portion of its oscillating trajectory, the probe takes photographs of the surface in the visible spectrum for comparison with known surface features. This gives the probe critical navigational information. When approaching an interesting site, the probe autonomously shuts its isolation valve permitting it to descend to the surface. As more and more of the landing snake comes into contact with the surface, the amount of mass which must be supported by the balloons gets smaller until the descent is gently arrested and the probe lands. While on the surface, various instruments collect data about the landing site. Despite very good insulation, the average surface temperature of $733°$ K slowly heats the probe and to avoid damage it must eventually open its isolation valve and return to the cooler upper atmosphere. Figure source is http://robotics.jpl.nasa.gov/tasks/aerobot/studies/venus.html.

9

Figure 1.3. An artist's conception of VFR above Western Eistla Regio (see Figure 5.15). The viewpoint is 1,100 kilometers (682 miles) northeast of Gula Mons at an elevation of 7.5 kilometers (4.6 miles). Lava flows extend for hundreds of kilometers across the fractured planes shown in the foreground, to the base of Gula Mons. The viewer looks to the southwest with Gula Mons appearing at the left just below the horizon. Gula Mons, a 3 km (1.86 mile) high volcano, has geographic coordinates of $\sim 22°$N, $359°$E. Sif Mons, a volcano with a diameter of 300 km (180 miles) and a height of 2 km (1.2 miles), appears to the right of Gula Mons. The distance between Sif Mons and Gula Mons is approximately 730 km (453 miles). The balloon material has a gold coating to resist the corrosive, sulfuric acid environment. The upper balloon provides primary lift and the lower balloon contains the reversible fluid. The rectangular box below the balloon contains the control system for the aerobot. The conical piece below that is the radio antenna and the circular sphere is the gondola. A solar panel dangles below, with a portion of the landing snake visible. Source: J. Balaram and K. Nock of NASA JPL, 1996. See http://robotics.jpl.nasa.gov/tasks/aerobot/studies/venus.html.

II. RELATED WORK

A. ROBOT MOTION PLANNING

The general subject of robot motion planning has been extensively researched in the last decade and the rate that significant results are found has been accelerating in the latter part of this time. However. the vast majority of work in this field addresses a special subset of robot motion planning problems that are of little relevance to the problem we consider in this thesis. Specifically, most work involves path planning for a two-dimensional robot like Sojourner attempting to avoid obstacles in navigating to a single goal. For example, Schwartz and Sharir [1988] survey a number of motion planning algorithms, but their focus is on planning collision-free movements between an origin and a single goal. Similarly, Krogh and Feng [1989] explore dynamically generating subgoals (way-points at vertices of polygonal obstacles) enroute to some single final goal. Other studies address analogous problems, sometimes with the added difficulty of an unknown terrain that requires mapping either before or during navigation [Durrant-Whyte and Cox 1990, Lumelsky *et al.* 1990, Rao 1992]. Some studies are slightly more relevant in that they consider this task in three dimensions vice two [Caddell 1991, Neto 1994]. However, relatively few articles consider planning for *multiple goals* in either two or three dimensions.

B. ORIENTEERING

Orienteering is a sporting game where several participants are given a compass and a map of some local terrain. Starting from a common location, their goal is to (1) navigate to several "control sites", (2) eventually arrive at a common destination having visited the largest number of the most valuable control sites, and (3) do so in the shortest time possible. Participants in the game are collecting points by visiting control sites. Some control sites might offer more points than others. Sometimes the game has a deadline (t_{max}). If participants do not arrive before the deadline, then they might either be charged a severe penalty in points or disqualified [Golden *et al.* 1987]. Orienteering is also referred to as the generalized traveling salesman problem (GTSP) [Tsiligirides 1984] and it has been shown to be an *NP*-hard problem [Golden *et al.* 1987]. This implies that a heuristic is probably the best approach for solving a large orienteering problem, however, smaller ones might be solved optimally in a reasonable amount of time.

When path planning for *multiple goals* is studied, the problem is usually considered to be some sort of orienteering. For example, Tsiligirides [1984] proposes two heuristic

algorithms for solving three orienteering problems based on the game. One of these is a stochastic algorithm that uses Monte Carlo techniques to randomly choose a large number of routes (with deterministic travel-times) from the set of all possible routes and then selects the best from these. The best route is based on a measure of desirability formed from the ratio of a site's score to the cost of reaching that site. The other is a deterministic algorithm that creates routes using a variant of the Wren and Holliday [1972] vehicle-routing procedure. This heuristic breaks a region into concentric circle sectors. Routes are created within sectors to minimize total travel times—they take the shape of a structure that looks similar to a flower petal. Tsiligirides then varies the radii of the circles and rotates their axes to examine 48 cases for each value considered for t_{max}.

In other research, Sposato [1995] solves an orienteering problem by finding optimal routes for the US Coast Guard's iceberg reconnaissance aircraft as they conduct the International Ice Patrol (IIP). This is an operation with the purpose of improving the navigational safety of ships in the North Atlantic by monitoring the limit of all known ice off the coast of Newfoundland. To solve the problem, he breaks the area of interest into a two-dimensional grid and implements it as a graph, $G = (N, A)$ where N is a set of nodes representing positions in the region and A is a set of arcs connecting the elements of N. Because Sposato models *aircraft* (capable of straight-line travel between any two points) flying through G, the possibility exists for his graph to be very dense ($|A| \approx |N|^2$) making optimal path planning a very computationally intensive task. However, he uses the IIP's operating procedures to limit the number of feasible paths through G, resulting in a very sparse graph. He then finds the optimal path through G by completely enumerating all feasible paths and returning the one with the highest reward value.

Golden *et al.* [1987, 1988] present algorithms that solve Tsiligirides' problems faster and better. These improved results rely on the use of a center-of-gravity heuristic. With this new heuristic, Golden *et al.* place extra importance on groups of sites that are clustered together. They accomplish this as follows. Using a "good" route, L, constructed with a computationally cheap heuristic, they evaluate the center-of-gravity of L as $g = (\overline{x}, \overline{y})$, where

$$\overline{x} = \frac{\sum_{i \in L} s(i)\, x(i)}{\sum_{i \in L} s(i)}, \tag{2.1}$$

$$\overline{y} = \frac{\sum_{i \in L} s(i)\, y(i)}{\sum_{i \in L} s(i)}, \tag{2.2}$$

and $s(i)$ is the score of a node, i with coordinates, $(x(i), y(i))$. After this, they calculate $a(i) = t(i, g) \quad \forall\, i \in N$, the time required to travel the straight-line distance from node i to

L's center-of-gravity, g. Using this information, they form a new route, L_1, by calculating the ratio, $r(i) = s(i)/a(i) \quad \forall\, i \in N$ and adding nodes to L_1 in decreasing order of $r(i)$ until no more nodes can be added without exceeding t_{max}. This is done iteratively, keeping the set of routes $R = \{L, L_1, L_2, \ldots, L_p, L_q\}$ until some L_p is identical to some L_q for $q > p$. Finally, the best route is chosen from R. This center-of-gravity heuristic consistently out-performs those of Tsiligirides.

In the aforementioned work, the authors all make an implicit assumption that distances between goals can be determined using standard Euclidean geometry. That is, if point A has coordinates (x_A, y_A, z_A), and point B has coordinates (x_B, y_B, z_B), then the distance between points A and B is merely $\sqrt{(x_B - x_A)^2 + (y_B - y_A)^2 + (z_B - z_A)^2}$. This is a completely valid assumption for the problems they consider, but is grossly inaccurate for the problem we solve.

Although aerobot path planning is clearly an orienteering problem, we cannot assume the distance between points of interest is Euclidean. Because an aerobot relies upon global wind patterns for horizontal mobility, distances along three-dimensional paths from one point to another involve several altitude changes and wind directions may be different at each altitude. This additional complexity unfortunately rules out the use of high-performance orienteering heuristics relying on a center-of-gravity approach.

Therefore, to address the unique issues involved in aerobot motion planning, this thesis relies on several heuristic and exact algorithms—generalized greedy path planning algorithms, Dijkstra's Algorithm, and partial and complete enumeration techniques [Ahuja et al. 1993, Cormen et al. 1990].

III. PROBLEM DESCRIPTION

Given a set of interesting sites on Venus, each with an associated scientific value, determine the optimal VFR path among them. The optimal path is the feasible path that collects the greatest cumulative scientific value within VFR's lifetime.

The problem divides into three smaller tasks: (1) construct a global circulation model (GCM) describing the Venusian environment; (2) create a practical aerobot model; and (3) plan the path for this aerobot model within the GCM.

A. VENUS GCM

Path planning requires a GCM of the Venusian atmosphere because VFR relies on global winds for horizontal movement. A simple GCM implementation consists of a graph where nodes represent three-dimensional position vectors, and arcs between nodes represent potential routes from one position to another.

As a result of numerous past exploratory missions to Venus and several studies using powerful Earth-based telescopes, scientists know many characteristics of the Venusian atmosphere [Hunten *et al.* 1983]. For example, it is clear that the atmosphere of Venus rotates faster than the solid planet by as much as two orders of magnitude; that the period of this rotation is about 4 days at the cloud tops; and that this rotation is strictly westward at all altitudes [Hou and Goody 1989]. Many more details are known (based upon repeated observation), but there is some debate regarding the *mechanisms* driving these circulation patterns [Gierasch *et al.* 1994, Hou and Goody 1989, Hunten *et al.* 1983, Limaye 1990, Linkin *et al.* 1986b, Moroz 1994, Newman *et al.* 1984, Rossow 1983]. Usually a proposed GCM explains these mechanisms—why various patterns occur in the atmosphere. However, the GCM used in this thesis makes no attempt at such explanation—instead, it is merely a simplified model with atmospheric characteristics similar to those observed. We list assumptions that highlight these simplifications below.

1. **Deterministic Characteristics**
   We assume that atmospheric characteristics are neither random nor dynamic and behave similarly to many recently proposed theories about their nature.

2. **Global Knowledge**
   We assume that a global, three-dimensional "map" of all pertinent characteristics (wind speed and direction, ambient temperature, etc.) of the GCM is available. An aerobot within this GCM knows everything it needs to know about the atmosphere at any position and altitude on the globe.

3. **Atmospheric Altitude**

   The upper boundary of the GCM occurs at an altitude of 70 km above the mean planetary radius (MPR) of 6.052 km. Characteristics of the atmosphere are most well known below this altitude and it is unlikely that an aerobot will fly higher. Based on current knowledge, that portion of the Venusian atmosphere above this altitude has little influence upon wind speeds and directions below [Hunten et al. 1983, Hou and Goody 1989].

4. **Variation of Zonal Wind Speed With Altitude**

   Based on all observations to date, the zonal wind is strictly westward at all altitudes, but variations in speed with altitude have been measured by the US Pioneer Venus and the Russian Venera probes. Vertical atmosphere profiles from Veneras 8, 9, 10, 12, and the Pioneer Venus probes shown in Figure 3.1 demonstrate this dependency and Figure 3.2 shows the corresponding GCM assumption.

5. **Variation of Zonal Wind Speed with Latitude**

   As shown in Figure 3.3, observational data indicate that zonal wind speed decreases with latitudinal distance from the equator at 70 km [Hunten et al. 1983, Keating 1990, Limaye 1990]. Figure 3.4 shows the GCM approximation of this behavior.

6. **Variation of Meridional Wind Speed with Altitude**

   A likely explanation for many Venusian atmospheric traits is that Hadley Cells span each hemisphere as shown in Figure 3.5. For this GCM, we assume that a single Hadley Cell is solely responsible for all dependence of meridional (North–South) wind speed upon altitude. It is well accepted that Hadley Cell circulation is the most prevalent mechanism driving meridional winds [Gierasch et al. 1994, Greeley et al. 1994, Hunten et al. 1983, Hou and Goody 1989, Moroz 1994], and this is weakly supported by measurements as shown in Figure 3.6.

7. **Variation of Meridional Wind Speed with Latitude**

   As mentioned above, strong evidence supports Hadley Cell circulation as the most prevalent process driving winds in the North–South direction. Figure 3.7 shows meridional wind observations on Venus, and Figure 3.8 shows the GCM assumption corresponding to these winds at an altitude of 70 km.

8. **Complete Absence of Vertical Winds**

   The Vega balloon experiment clearly measured significant vertical winds on Venus [Linkin et al. 1986a, Sagdeev et al. 1986b]. However, the winds—mostly downdrafts at velocities as large as 3 m/s—occurred at sporadic intervals and the data is noisy and insufficient for adequate prediction. Therefore, the GCM assumes only horizontal winds exist.

9. **Atmospheric Characteristics**

   There are some characteristics of the atmosphere not directly related to wind

speeds and directions that are nonetheless important to model. One such characteristic is atmospheric temperature. It is used for modeling heat transfer between atmosphere and aerobot electronics so that instrument temperature limits are not exceeded.

B. AEROBOT MODEL

The aerobot model addresses only thermal concerns. The atmosphere is very hot at low altitudes and much cooler at high altitudes (see Figure 3.9). If an aerobot spends too much time at lower altitudes, it can overheat resulting in damaged electronics. Therefore, careful consideration of heat transfer into and out of the aerobot is critical.

Heun [1996] provides a simple but adequate method for modeling heat transfer that assumes aerobot heat absorption occurs according to the following equations:

$$Q = \int_{t_0}^{t_f} q \, dt \, ; \tag{3.1}$$

$$q = \sigma S e (T_o^4 - T_i^4) \, ; \tag{3.2}$$

$$S = 4\pi r^2 \, . \tag{3.3}$$

Here Q is the total heat absorbed in Joules during the time interval between t_0 and t_f, q is the heat transfer rate into the aerobot gondola in Joules per second, σ is the Stefan-Boltzmann constant for radiative heat transfer, and S is the surface area in square meters of the inner of two spheres that make up the gondola. The electronics are within this inner sphere—the volume between the outer and inner spheres is vacuum insulated. Effective emissivity between the two spheres is represented by e, a unit-less quantity. T_o is the temperature of the outer sphere in degrees Kelvin. We assume this is always at the ambient temperature of the immediate surroundings. T_i is the temperature of the inner sphere, kept constant by a phase change material (lithium nitrate) present for just that purpose, and r is the radius of the inner sphere.

Equation (3.1) is a general way of determining total accumulated heat, Q, based upon some known heat transfer rate, q. Equation (3.2) is the radiative heat transfer equation and Equation (3.3) gives the surface area of a sphere based upon its radius.

The design of the aerobot gondola includes a reflux heat pipe with very low thermal conductivity for heat flow *into* the gondola (heat absorption occurs very slowly), and very high thermal conductivity for heat flow *out of* the gondola (speedy heat rejection) [DiCicco *et al.* 1995]. The heat pipe's low conductivity for absorption results in the major heat leak

17

into the gondola being due to radiation from the outer sphere to the inner sphere. The absorption rate from thermal radiation is so much larger than all others that it is safe to treat all other heat leaks into the gondola as insignificant [Heun 1996]. Thus, Equation (3.2) is the best way to predict q.

The inner sphere of the gondola contains an aerobot's temperature sensitive electronics and a quantity of lithium nitrate phase change material (PCM). Lithium nitrate melts at about 30° Celsius or 303° Kelvin. As is true during a phase change of any material, the temperature of the material remains constant until all of it has undergone the phase change. The amount of heat energy that must be absorbed to change the state of a material from solid to liquid is known as its latent heat of fusion, L_f. The latent heat of fusion of lithium nitrate is about 75% that of water, or $L_{f_{PCM}} = 250$ kJ/kg. The inner gondola will most likely contain about 3 kg of lithium nitrate so the PCM can absorb a maximum of ~750 kJ of heat energy before its temperature will rise above 30° C. To keep an aerobot's electronics at a safe and stable temperature during excursions into the very hot lower atmosphere of Venus, an aerobot should begin its ascent toward the cool upper atmosphere (where it can reject this accumulated heat) by the time it absorbs about 50 to 75% of its heat absorption limit [Heun 1996].

Heat transfer rates depend upon the temperature difference between the heat source and heat sink. The highest expected altitude for an aerobot is 60 km [DiCicco *et al.* 1995], and based on data collected by the Magellan mission, the temperature at this altitude is about 240° K [Twicken 1996]. Since the PCM is always at about 303° K, this is a relatively small temperature difference driving heat transfer out of the aerobot gondola. In fact, it is clear from Figure 3.9 that heat rejection can only take place between about 55 and 60 km, so only about one quarter of each oscillation permits heat rejection. Fortunately, during the other three quarters of each oscillation period, very little heat absorption occurs. Despite the marginal conditions for heat rejection while oscillating about the EA, the heat pipe is so effective that all heat absorbed in the lower atmosphere can be rejected very quickly in the upper atmosphere. An aerobot can reject 750 kJ of heat energy by spending a duration of about 8 hours in the upper atmosphere, oscillating about its EA [Heun 1996].

C. PATH PLANNING APPROACH

Once a reasonably realistic representation of the Venusian global environment and a simple model of an aerobot are implemented, we solve the path planning problem. Since our assumptions state that the characteristics of the GCM are static with respect to time, and that a global "map" of all relevant atmospheric properties is available for

use in planning, what remains is a simple orienteering problem [Golden *et al.* 1987, Golden *et al.* 1988, Tsiligirides 1984]. This perfect knowledge problem is useful as a best-case planning benchmark—the most optimistic situation an aerobot faces in its mission.

1. Problem Formulation

Similar to Sposato [1995], we use a graph, $G = (N, A)$ to model the GCM. In our case, however, the set N contains nodes representing *three*-dimensional position vectors. The set A contains all directed arcs, (i, j), in the graph representing allowable aerobot travel directly from node $i \in N$ to node $j \in N$. Using this model, the entire three-dimensional problem domain consisting of all altitudes from the planetary surface to the upper boundary of the atmosphere, and all latitudes and longitudes divides into $|N|$ nodes—each representing a non-zero volume of space—together representing all possible positions that the aerobot can occupy. The set, N', is the proper subset of N, $N' \subset N$, consisting of all scientifically interesting sites on the surface of Venus as well as the atmosphere insertion point where the aerobot enters the GCM from orbit.

An important property of the arcs in A is that they capture the prevailing wind direction at the node from which the arc originates: an aerobot's only means of horizontal mobility relies on the wind. These arcs may also have a vertical component resulting from upward or downward motion induced by aerobot buoyancy changes. Also, aerobot travel time, $t_{(i,j)}$, along an arbitrary arc $(i, j) \in A$, depends upon the local wind speed at node i, where the arc originates.

Below we list a mathematical programming formulation for determining the three-dimensional path that VFR should use to explore a subset of N' with the largest quantity of time-weighted scientific data within its lifetime. It relies on forming a subgraph, $G' = (N', A')$ where A' contains directed arcs connecting pairs of nodes in N'. In other words, an arc $(i, j) \in A'$ represents a path of potentially many arcs in A. Chapter IV describes the method we use to form this set of paths. The problem formulation is done in the Naval Postgraduate School Standard Format.

1. **Indices**

   i, j: Elements in the set, N'. Nodes are numbered using consecutive non-negative integers starting at 0. An ordered pair of distinct indices represents an element of the set, A'. The first index is the "from" or *leaving* node, and the second is the "to" or *landing* node, so that the ordered pair (i, j) is the directed arc from node i to node j. Variables and data values subscripted with these indices represent the attributes associated with an arc or a node as appropriate.

2. **Data**

   n_{ip}: The node representing the atmosphere insertion point—the location where the aerobot enters the Venusian atmosphere.

   n_f: The last node the aerobot visits is a dummy node corresponding to the position where the aerobot "dies".

   u_i: The time-related value associated with visiting node i has units of "research-value"/second. Equation (3.4) below uses it as a penalty for each second's delay in visiting node i.

   v_i: The scientific value associated with visiting node i has units of "research-value".

   $m_{i,j}$: A large constant with units of seconds.

   $t_{i,j}$: The time required to transit arc (i,j) in seconds. For all $i \in N'$, the arc, (i, n_f) has transit time, $t_{i,n_f} = 0$.

   L: The operational lifetime of the aerobot in seconds, from the time of deployment in the target planet's atmosphere at n_{ip}.

3. **Decision Variables**

   $x_{i,j}$: A binary variable with value 1 if the aerobot traverses arc (i, j) and 0 otherwise.

   y_i: A continuous variable corresponding to the time the aerobot visits node i. This variable gives the formulation an aspect of time passage—the idea that visiting node i at one time is a different event than doing so at another time. It has units of seconds.

4. **Formulation**

   Maximize:

$$\sum_{(i,j)\in A'} v_j\, x_{i,j} \quad - \quad \sum_{i\in N'} u_i\, y_i \tag{3.4}$$

20

Subject to:

$$\sum_{(i,j)\in A'} t_{i,j}\, x_{i,j} \leq L \tag{3.5}$$

$$\sum_{i:(i,j)\in A'} x_{i,j} \leq 1 \qquad \forall\, j \in N' \tag{3.6}$$

$$\sum_{i:(j,i)\in A'} x_{j,i} \leq 1 \qquad \forall\, j \in N' \tag{3.7}$$

$$\sum_{i:(i,j)\in A'} x_{i,j} - \sum_{i:(j,i)\in A'} x_{j,i} = 0 \qquad \forall\, j \in N' \tag{3.8}$$

$$\sum_{j:(n_{ip},j)\in A'} x_{n_{ip},j} = 1 \tag{3.9}$$

$$\sum_{i\in N'} x_{i,n_f} = 1 \tag{3.10}$$

$$y_i + t_{i,j}\, x_{i,j} \leq y_j + m_{i,j}(1 - x_{i,j}) \qquad \forall\, (i,j) \in A' \tag{3.11}$$

$$x_{i,j} \in \{0,1\} \qquad \forall\, (i,j) \in A' \tag{3.12}$$

$$y_i \geq 0 \qquad \forall\, i \in N' \tag{3.13}$$

$$y_1 = 0 \tag{3.14}$$

2.   Discussion of Formulation

The objective function, Equation (3.4), provides the total scientific value collected (both time-weighted and time-independent). Equation (3.5) limits the aerobot's exploration time to no more than its lifetime. Equation (3.6) allows at most one leaving node for each landing node and Equation (3.7) allows at most one landing node from each leaving node. Equation (3.8) is a continuity of path constraint. Equation (3.9) requires the path to start at n_{ip}, and Equation (3.10) forces the aerobot to stop exploring when it dies at n_f. Equation (3.11) prevents sub-tours (circular paths) that result in eventually landing on a previously visited node. Equation (3.11) also associates a time-of-visit with each node, thereby establishing a history anchored in real-time. The resulting path found by solving this formulation is then described by a series of nodes, $\{n_{(0)}, n_{(1)}, n_{(2)}, \ldots\}$ and times that each node in the series was visited, $\{y_0, y_1, y_2, \ldots\}$ from j and y_j in that equation. Equations (3.12), (3.13), and (3.14) constrain the decision variables' domains.
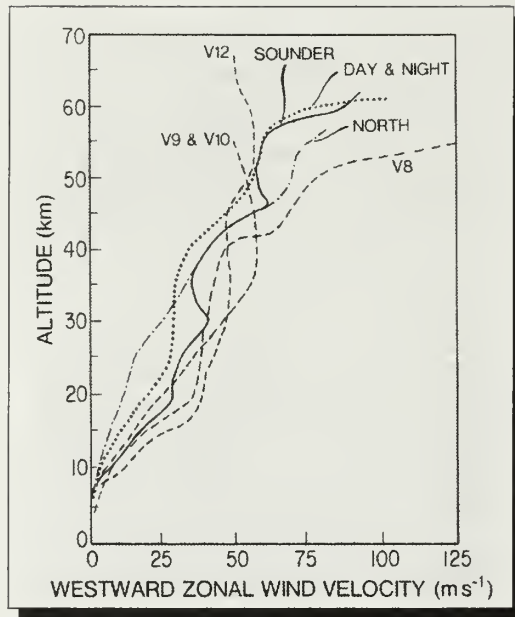
Figure 3.1. Vertical profiles of east-to-west wind speed from Doppler tracking of Veneras 8, 9, 10, 12 (V8, V9, V10, V12) and interferometric tracking of Pioneer Venus probes (Sounder, North, Day & Night). See Figures 5.13 and 5.14 for locations of these probes. Source: [Hunten *et al.* 1983].
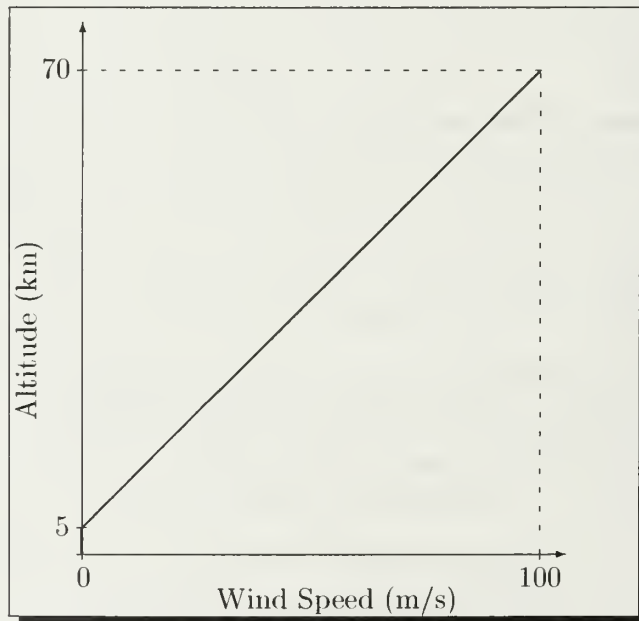
Figure 3.2. Zonal wind speed as a function of altitude for the GCM of Venus.
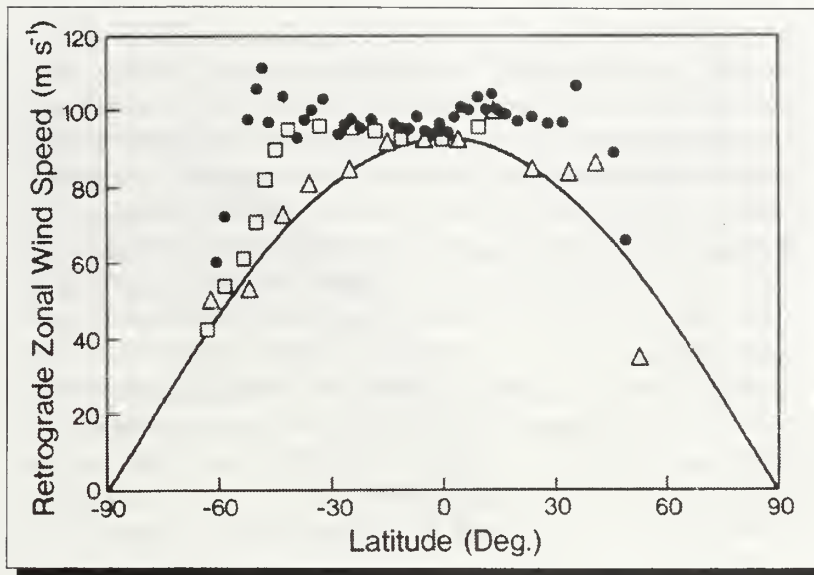
Figure 3.3. Longitudinally averaged retrograde zonal wind velocities versus latitude, inferred from the tracking of small-scale cloud features (probably at an altitude near 75 km) in spacecraft ultraviolet images of Venus. The solid curve is the zonal wind velocity for solid body retrograde rotation with equatorial speed of 92.4 m/s corresponding to a period of 4.8 days. Source: [Hunten *et al.* 1983].
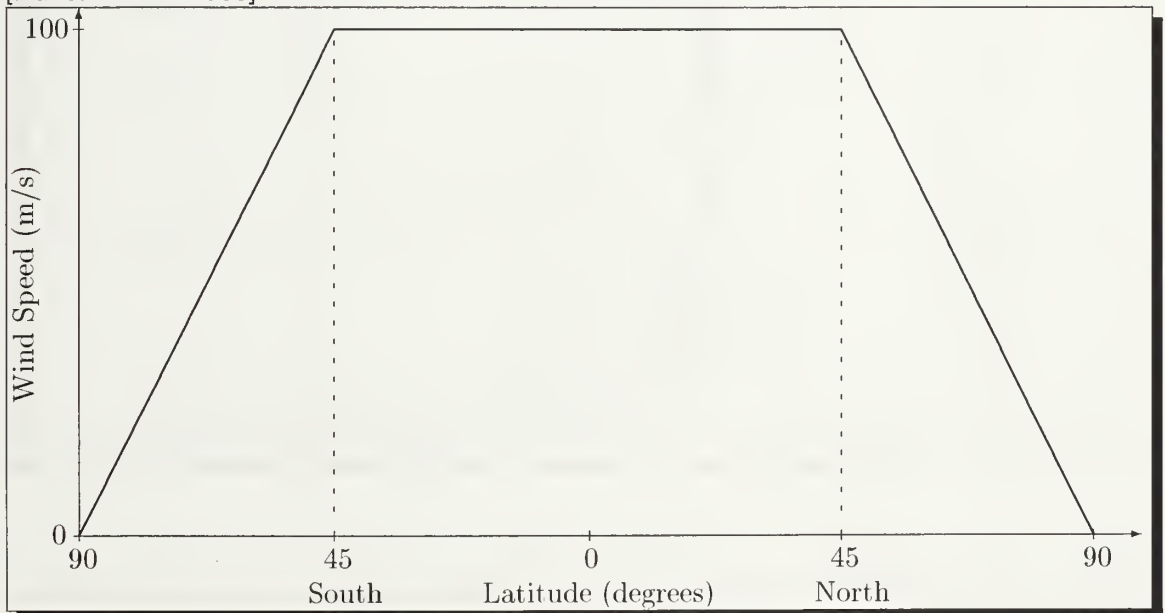
Figure 3.4. Zonal wind speed variation with latitude at an altitude of 70 km for the GCM of Venus.

HYPOTHETICAL
LOWER ATMOSPHERE
HADLEY CELLS
AND INDIRECT CELLS

CLOUD LEVEL
HADLEY CELL

WESTWARD
SUPERROTATION
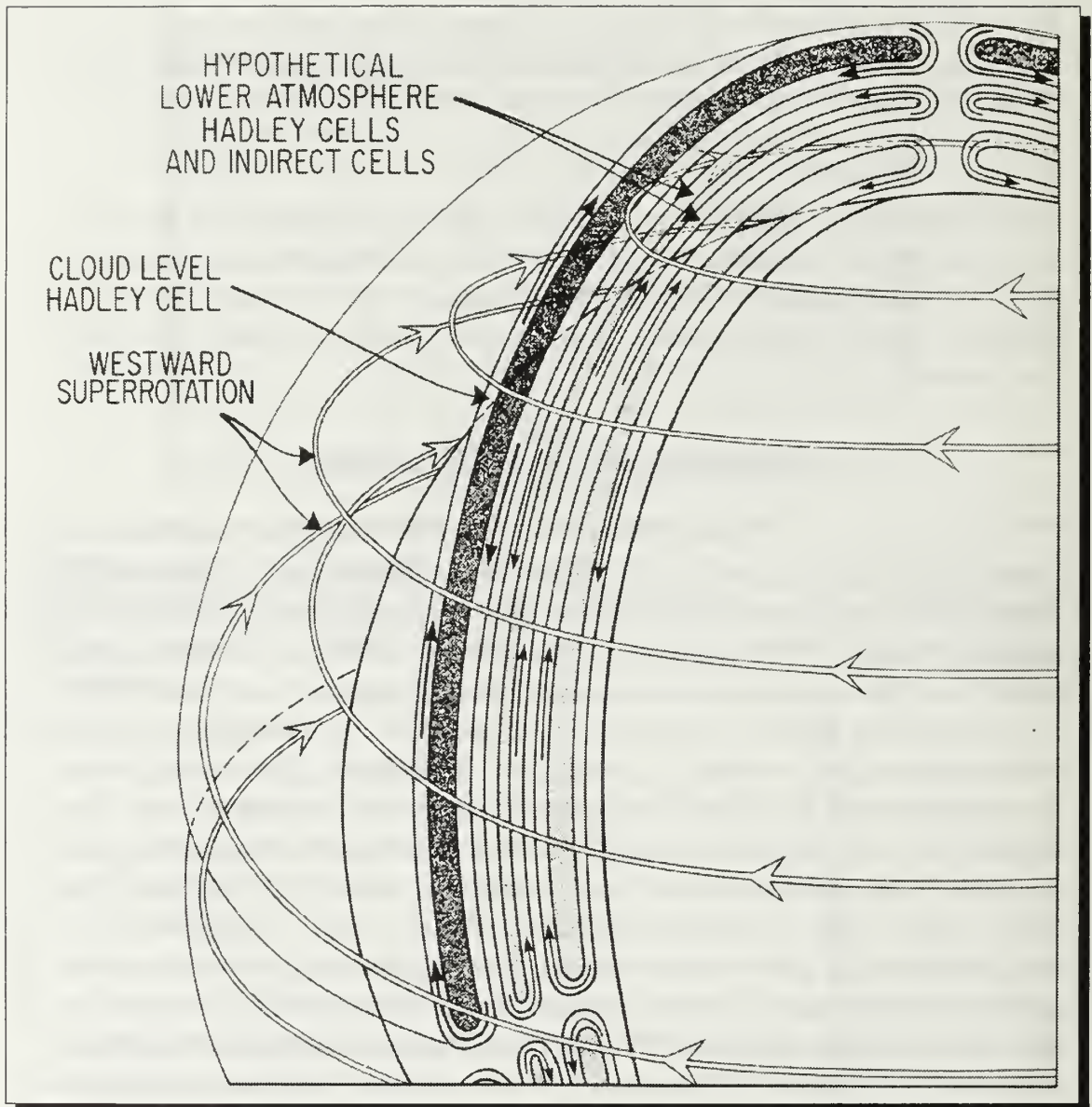
Figure 3.5. Cloud-level Hadley Cell carrying the excess radiative energy deposited at high altitudes in the equatorial region to polar latitudes. Below the clouds, there is probably a series of alternating direct and indirect meridional cells including, a ground-level Hadley Cell. Source: [Hunten *et al.* 1983].
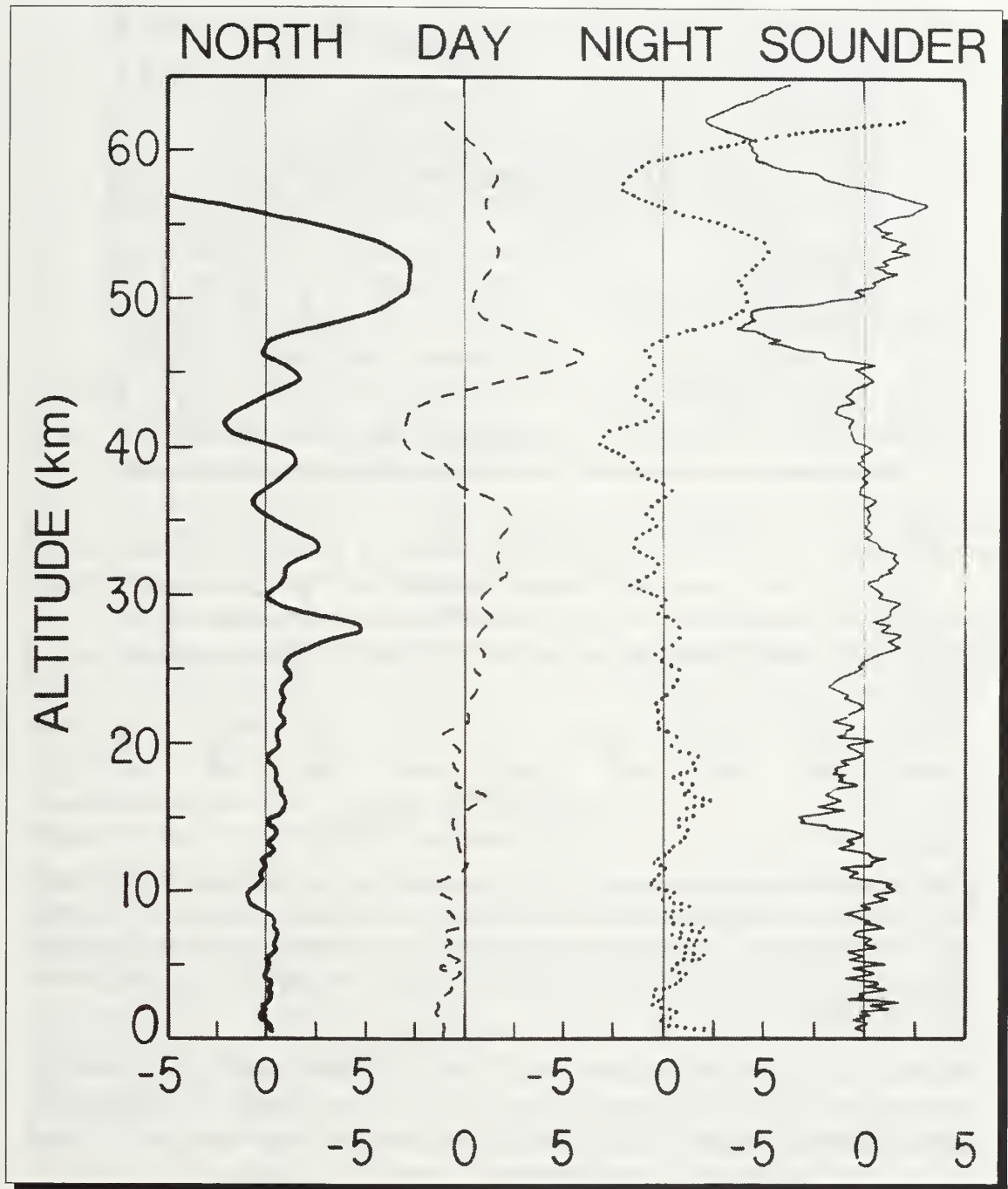
Figure 3.6. Meridional wind velocity profiles from interferometric tracking of the Pioneer Venus probes. See Figures 5.13 and 5.14 for locations of these probes. Source: [Hunten *et al.* 1983].
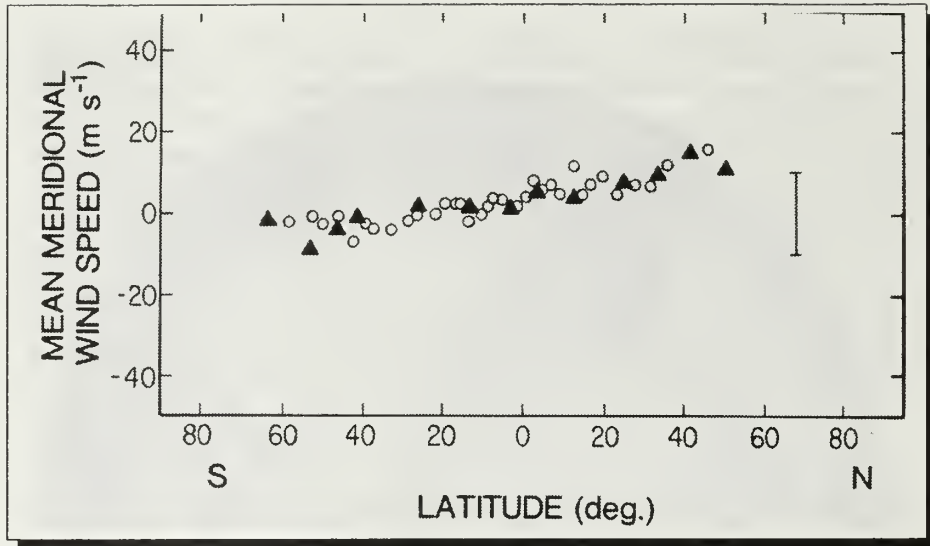
**Figure 3.7.** Time and longitudinally averaged meridional wind speeds from tracking of small-scale cloud features (probably at an altitude near 75 km) in spacecraft ultraviolet images of Venus. The vertical error bar is a representative rms deviation of the measurements about the plotted means. Positive speeds in northern latitudes are northward motions; negative speeds in southern latitudes are southward motions. Source: [Hunten *et al.* 1983].

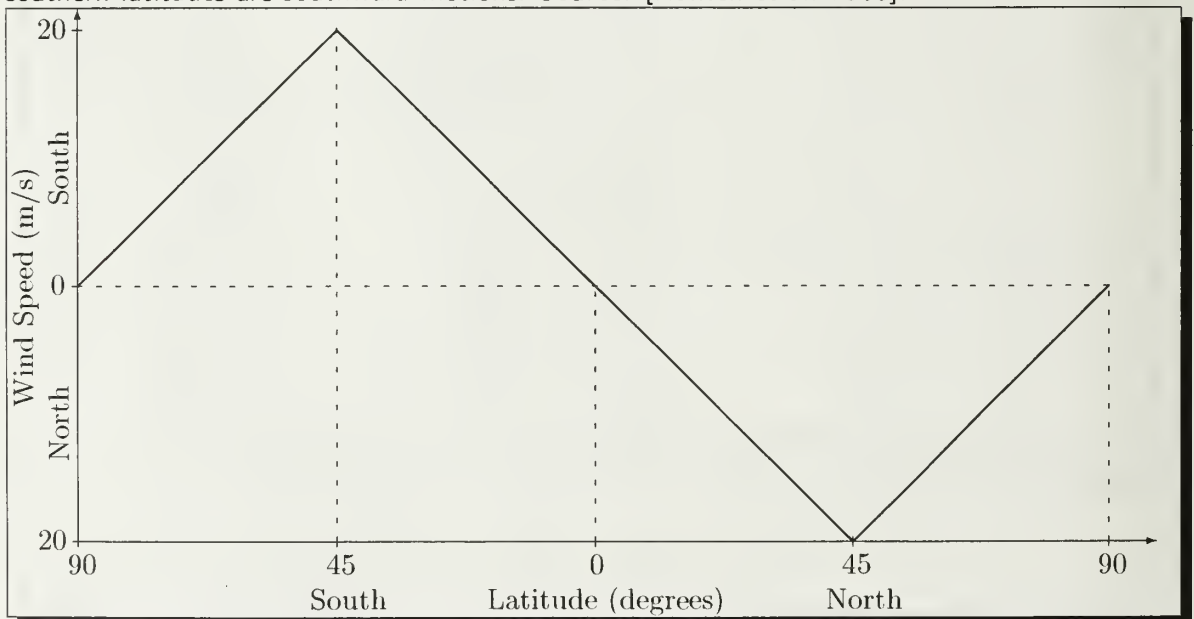**Figure 3.8.** Meridional wind speed as a function of latitude at an altitude of 70 km for the GCM of Venus. North implies winds blowing *to* the North.
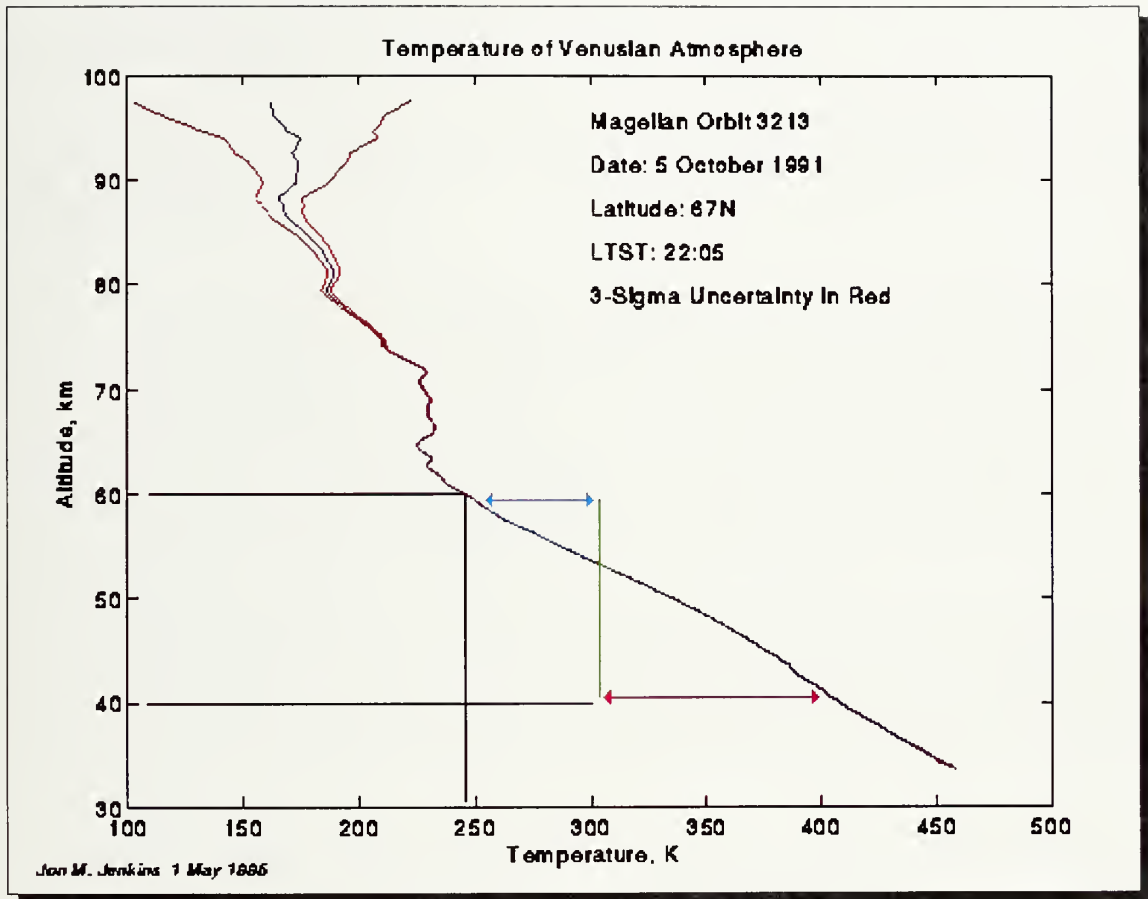
Figure 3.9. Temperature changes dramatically as a function of altitude in the Venusian atmosphere. The melting point of the lithium nitrate phase change material within the inner sphere of the gondola is $303°$ K, shown by the vertical green line. The largest temperature difference driving heat *rejection* from the gondola is $\sim50°$ K at 60 km. The cyan-colored, double-headed arrow represents this difference. VFR oscillates between 40 and 60 km in altitude (shown by the horizontal black lines), so heat rejection can only occur in the upper 5 km of that range. Although the aerobot cannot *shed* heat in the lower 15 km of this range, it absorbs very little heat here. This is due to the reflux heat pipe's effectiveness and the relatively small temperature difference (magenta-colored, double-headed arrow) driving heat absorption at this altitude. For comparison's sake, the planetary surface is at an average of $733°$ K, and the resulting temperature difference is $430°$ K. VFR can reject ~750 kJ of heat energy by oscillating about its EA for 8 hours. Source: Jan M. Jenkins, 1996 (See http://nova.stanford.edu/projects/mgs/images/t3213.gif).

IV. ALGORITHM DEVELOPMENT

A. STRUCTURE OF GCM

We generate the graph, $G = (N, A)$ (representing the GCM), with a computer program written in C++ called *vgcm* for "Venus Global Circulation Model". G has a very well defined structure:

1. It has a discrete set of altitudes. We adjust the number of altitudes using an input parameter, P_ρ. These altitudes range from the planetary surface, altitude 0 (a_0), to the upper boundary of the GCM at 70 km above the MPR. The altitudes occur at equally spaced intervals. The size of the interval depends only upon the number of altitudes and the upper boundary of the GCM. For example, in most problems we solve, G has 9 altitudes. They start at 0 km above MPR, and each successively higher altitude is 8.75 km above the last until the top-most altitude, altitude 8 (a_8) is reached at 70 km above MPR.

2. It has a discrete set of latitudes. We adjust the number of latitudes using an input parameter, P_ϕ. The northern- and southern-most extent of these latitudes are two other input parameters to *vgcm* and G typically includes latitudes within ~30° of the equator. These latitudes are equidistant and the spacing between them is a function of the number of latitudes chosen and the size of the latitude range.

3. It has a discrete set of longitudes. We adjust the number of longitudes using an input parameter, P_θ. These longitudes completely cover the planet so that circumnavigation of Venus within G is possible. They are equidistant and their spacing depends only upon the number of longitudes chosen.

4. The combination of longitude, latitude, and altitude uniquely specify any node in G.

5. There are at most three directed arcs emanating from any node in G. One arc represents an upward step in altitude, another represents a downward step in altitude, and another represents no altitude change by the aerobot.

6. In addition to the vertical dimension, every directed arc, $(i, j) \in A$, represents one westward step in longitude as well as a *possible* latitude change. We use a single Hadley Cell circulation pattern (see Figure 3.5) to determine the amount of this latitude change. The middle altitude has winds that are due west and directed arcs with landing nodes at the middle altitude have no latitude change. In the upper half of the altitude range, winds have a pole-ward component that is one latitude-step larger with each higher altitude. In the lower half,

winds have an equator-ward component that is one latitude-step larger with each lower altitude. For example, if G has 9 altitudes, $\{a_0, a_1, a_2, \ldots, a_7, a_8\}$, then the middle altitude, a_4, has due westerly winds, the wind direction at a_5 carries an aerobot one step west in longitude with a latitude change that is one step in the pole-ward direction (north in the northern hemisphere, south in the southern hemisphere), the wind direction at a_6 carries an aerobot one step west in longitude with a latitude change that is *two* steps in the pole-ward direction, a_7 winds have a *three* step latitude change in the pole-ward direction, and a_8 winds have a *four* step latitude change in the pole-ward direction. The lower half of the altitude range is symmetric to the upper half with latitude changes that are equator-ward (north in the southern hemisphere, south in the northern hemisphere).

7. Nodes in G might have fewer than three directed arcs leaving them because of a GCM boundary such as the top-most or bottom-most altitude.

8. We find the landing node of an arc leaving some specified node with an *upward* altitude step using the prevailing wind direction one altitude *above* the leaving node. Similarly, we get the landing node of an arc leaving a node with a *downward* altitude step from the prevailing wind direction one altitude *below* the leaving node. Finally, we determine the landing node of an arc leaving some node with *no* altitude change from the prevailing wind direction *at* the leaving node. Wind directions at each altitude depend upon (1) the resolution of the GCM (as set by P_ρ, P_ϕ, P_θ), and (2) a simplification of currently understood global wind patterns on Venus.

See Figure 4.1 for a graphical description of G.

B. PATH PLANNING

The aerobot starts at node, $n_{ip} \in N'$, representing the atmosphere insertion point and this is the origin of the first trip. Subsequent trips to interesting sites originate at the previous trip's destination. The ultimate goal is to determine an efficient route for aerobot travel among all the interesting sites in the GCM.

We begin to solve this problem by finding efficient routes for travel from any one interesting site, $i \in N'$, to any other interesting site, $j \in N'$, through the graph, $G = (N, A)$. The ideal solution to this single-goal problem is to use the shortest path for travel between two interesting sites. We use a modified Dijkstra's Algorithm [Cormen *et al.* 1990] for this task.

1. Dijkstra's Algorithm

We find a short (but not necessarily the shortest) path between any two nodes, $i, j \in N$ with a slightly modified Dijkstra's Algorithm. The sole modification—a rule necessary for more realistic aerobot motion modeling—forces upward motion to be the only option available to the aerobot once it has chosen to move upwards and until it reaches its EA. The reversible fluid buoyancy control system is the source of this rule. Thermodynamic characteristics of the Venusian atmosphere and the aerobot's reversible fluid require that once the aerobot has chosen to travel upwards (by opening the isolation valve to the fixed-volume pressure vessel) it will remain positively buoyant until it reaches its EA. At this time, the evaporation/condensation negative feedback cycle restores the aerobot's freedom to remain at its current altitude or descend again.

Generally speaking, Dijkstra's Algorithm guarantees an optimal shortest path between a source node, s, and all other nodes as long as the graph contains no negative-cost arcs [Cormen *et al.* 1990]. Although $G = (N, A)$ meets this requirement with aerobot travel time $(t_{i,j})$ as the arc costs, we cannot guarantee an optimal shortest path due to the way we implement our upward motion restriction. Specifically, Dijkstra's Algorithm uses only one node label corresponding to the shortest known distance to the node and explores nodes by choosing the node with the smallest known distance in its priority queue. We maintain this single node label in our modification and add a new requirement based on a portion of the path's history. Doing so introduces the possibility of missing the shortest path between s and some other node, t. To see this, assume our modified Dijkstra's algorithm identifies a shortest path between s and t and this passes through node i. The optimality of Dijkstra's algorithm relies on the shortest path from s to i being part of a shortest path from s to t. This may not be satisfied due to the additional restriction our modification uses. Specifically, say the shortest trip to i occurs while going up, thus upward motion must continue afterwards until reaching EA. There may be a longer path to i going downwards (thus having no subsequent motion restriction) that is nonetheless part of a *shorter* path to t than the path going upwards through i. This shorter path to t cannot be found by our modified Dijkstra's algorithm because the longer path to i is never explored. The modified Dijkstra's Algorithm therefore cannot guarantee an optimal path.

In planning the best path for VFR to travel among interesting sites on Venus, we first run our algorithm on $G = (N, A)$ with each node $i \in N'$ as a starting node. Each run yields a path from the starting node for that run, $i \in N'$, to every other node, $j \in N'$, if such a path exists. In this manner, we add arcs, (i, j) to the set, A'. If no path exists from $i \in N'$ to $j \in N'$ through $G = (N, A)$, then the arc, (i, j) is not added to A'. When

checking for the existence of arcs. $(i, j) \in A'$, we also determine the arcs' characteristics such as travel time, $t_{i,j}$, from $i \in N'$ to $j \in N'$ along the path through $G = (N, A)$. Prior to these runs. we know the elements of N', but have no knowledge about what arcs exist in A'. After running our algorithm for each node, $i \in N'$, we know the elements of A' and the characteristics of those elements. Thus, we now know all details of the graph, $G' = (N', A')$, and this graph contains a summary of G consisting only of that information important for the next task—multiple-goal path planning.

2. The Orienteering Problem

Except for arriving at a specified destination, an aerobot is basically the sole participant in an orienteering game with the entirety of Venus as its terrain. Instead of competing against other participants, an aerobot is competing against time because the robot can withstand the harsh Venusian environment for only a limited (but unknown) duration.

In G'. we have all the information we need to solve this orienteering problem. We solve it in a number of different ways using a C++ computer program called *CarpeDiem*, for the idea is, in fact, to "seize the day!"—to live life to its fullest. It is vitally important for planetary scientists to get as much as possible out of an aerobot's life.

In finding an efficient route through G', *CarpeDiem* uses a ratio similar to Tsiligirides' [1984] measure of desirability. It is the ratio of a site's scientific value to the time spent reaching it from the aerobot's current location. We refer to this ratio as the "value-to-time ratio". *CarpeDiem* uses three different algorithms in planning a route through G', and in each one, its goal is to maximize the total value-to-time ratio of the route.

One is a very greedy algorithm that looks only one step into the future and decides what interesting place to visit next based upon the value-to-time ratio of all single-step trips that are feasible from the aerobot's current location. This one step heuristic is a very short-sighted algorithm in that it might overlook high-value routes through a large number of low-valued sites that are clustered together.

Another is a slightly farther-sighted algorithm that looks at the value-to-time ratio of all two-step trips that are feasible from the aerobot's current location and uses this to decide what site to visit next.

The third algorithm finds an optimal solution to the problem of orienteering through G'. This algorithm uses the method of checking *each* distinct path through G' that visits all feasible nodes $i \in N'$ for its value-to-time ratio. It then returns the path with the largest result. Because completely enumerating all distinct paths through G' is exponential in N', use of this algorithm is only practical if N' has a dozen or fewer elements. To completely enumerate all distinct paths among 13 interesting sites requires approximately 31 hours on an IBM RS 6000 Model 590.
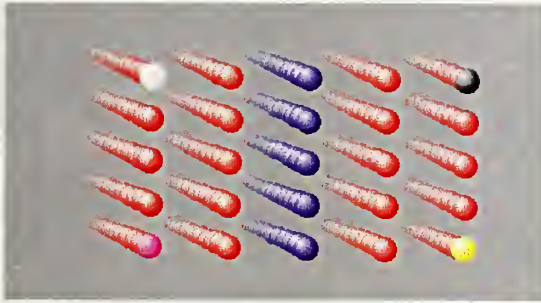
(a) Slightly offset forward view looking directly downwind or westward. Southward is to the left.
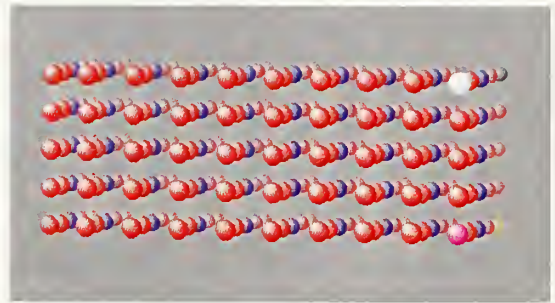
(b) Slightly offset side view looking northward. Westward is to the left.
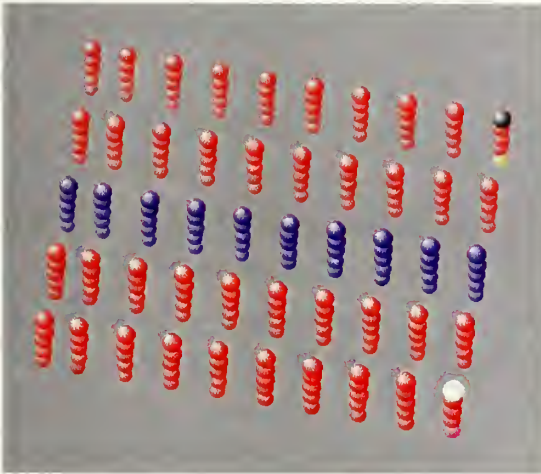
(c) Slightly offset top view looking downward. Westward is to the left.

(d) A three-dimensional perspective looking downward and to the northwest.

Figure 4.1. A typical Global Circulation Model (GCM). This is a Mercator projection of the spherical shape of the GCM with an additional vertical dimension to represent altitude. Note that a Mercator projection distorts dimensions by an amount proportional to their distance from the equator so features at high latitudes appea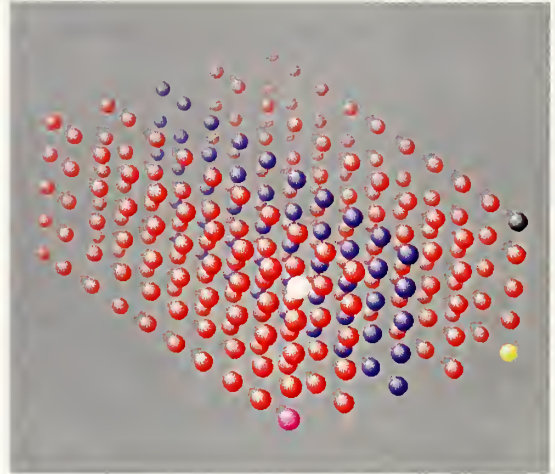r to occupy more area than they actually do. Also note that we show longitudes of the GCM in °W rather than the more usual °E as in Figures 5.13 and 5.15. The colored spheres represent nodes. Most nodes are red, but equatorial nodes are blue and other colors are at the corners of the GCM's prime meridian (0°W). Magenta is at the bottom southeast corner, white is at the top southeast corner, grey is at the top northeast corner, and yellow is at the bottom northeast corner. This GCM spans the entire range of longitudes, from 0°W to 350°W at 10° intervals, has a latitude band from 30°S to 30°N at 0.5° intervals, and contains nine altitudes. For visual clarity, we show only a fraction of all nodes.

V. RESULTS OF PATH PLANNING

A major concern in the development of computer programs to solve aerobot path planning problems is the computational performance of these programs. The task of modeling the atmosphere of an entire planet with even a moderate resolution is normally done on a supercomputer. Such hardware was not readily available for the work involved in this thesis so we devote effort to ensuring that problem run-times are not excessive for computers with modest resources.

Except for a 13-site problem that required 31 hours of run-time on an IBM RS 6000, all problems were run on a 75 MHz Pentium personal computer (PC) with 32 MB of random access memory (RAM). For problems with less than 12 interesting sites, total cumulative run-times using all three path planning algorithms are less than five minutes on the PC.

A. GCM RESOLUTION

As mentioned earlier, accurate modeling of temperature considerations is very important to this problem. However, we make two unrealistic assumptions regarding thermal modeling in all problem solutions in this Chapter.

The first assumption is that VFR's maximum heat absorption limit is 100 to 200 times larger (depending upon GCM resolution) than its realistic value of $\sim$750 kJ. We use this assumption because computer memory resources limit the resolution of a GCM that *CarpeDiem* can solve. We estimate that without extensive reprogramming, achieving $\sim$100 times higher resolutions requires $\sim$100 times more RAM. The highest resolution GCM that *CarpeDiem* can solve running on available hardware has $\sim$32 km between successive latitudes and $\sim$211 km between successive longitudes. These numbers represent the smallest distinguishable distances in G, and they are not small enough to allow realistic thermal modeling—VFR absorbs roughly half of its actual heat limit in traveling a distance represented by just one of these steps near the surface of Venus. This departure from realistic thermal modeling is unfortunate, but *CarpeDiem* can still be used by mission planners to find general aerobot paths for missions at Venus.

The second assumption is that instead of performing a heat transfer calculation and deciding how next to proceed at every node $i \in N$ along a path, we check for violation of thermal constraints at each node $i \in N'$ by adding up the total heat absorbed over the course of each trip. If a trip violates the thermal constraint, then we assume VFR requires an additional four days (one circumnavigation in the high-speed winds at EA) to first cool off and then make the trip (see Figure 5.8). We then reset the aerobot's heat-load

just prior to embarking on the next trip. This assumption does not limit the usefulness of our solutions since each trip is as short as the modified Dijkstra's Algorithm can produce (although this is not necessarily an optimal shortest path). If some trip, $(i, j) \in A'$ violates the aerobot's thermal limit, we can be sure that no shorter path between i and j can be found by *CarpeDiem*. Thus, *any* trip starting at i and ending at j that does not overheat the aerobot must include at least one planetary circumnavigation to allow aerobot cooling, and we include this time in the solution.

B.   GENERATING INTERESTING SITES

Path planning for VFR requires that we first identify the interesting sites in G. We give *CarpeDiem* two different capabilities for this. It either generates interesting sites randomly or reads them from a file supplied by the user. This way, planning is easily adaptable to many different missions for different aerobots—each with its own set of interesting sites. In the following sections, we use all three of *CarpeDiem*'s algorithms to plan routes for several small example missions and use the two heuristics to plan routes for a prototypical mission that explores numerous interesting sites recently documented in the planetary geology literature [Head *et al.* 1996]. In each case, the algorithms attempt to maximize the objective function value in Equation (3.4) and find the path with the maximum research-value per time invested.

C.   EQUAL PRIORITY SITES

We first find a path through several sites of equal priority with $u_i = 0 \quad \forall\, i \in N'$. Table 5.1 shows the sites' coordinates and research-values. Path planning through equally interesting sites permits a clear focus on the other issue (travel time) that guides the basic decision faced by VFR. As expected, in the one-step algorithm (Table 5.2), *CarpeDiem* directs VFR to the nearest (in time, not distance) interesting site in every decision. While slightly different from the one-step heuristic's results, the two-step algorithm also tries to minimize travel time in visiting all interesting sites (Table 5.3). Table 5.4 shows the optimal path found by completely enumerating all distinct paths among the interesting sites and choosing the one with the largest value-to-time ratio. Since all sites have equal value, this is the route through all sites with the shortest travel time.

D.   VARIED PRIORITY SITES

A more likely mission contains sites with a range of priorities. Table 5.5 depicts the problem shown above—the same seven interesting sites with $u_i = 0 \quad \forall\, i \in N'$—but

Site	θ (°W)	ϕ (°N)	Value
n_{ip}	70	−13.5	0
n_1	200	−8.5	5,000
n_2	210	1.5	5,000
n_3	90	4.5	5,000
n_4	320	11.5	5,000
n_5	330	10	5,000
n_6	240	10.5	5,000
n_7	120	18.5	5,000

Table 5.1. In this problem, all interesting sites in N' have equal priority (as evidenced by their identical research-values). θ and ϕ are typical measures of longitude and latitude with one important exception: θ is in °W vice the usual °E as in Figures 5.13 and 5.15. Both figures show rough physical locations of these sites with respect to other planetary features, but the reader should remember to convert from °W to °E (°E = $|\theta - 360°|$) before indexing their abscissas.

Trip	Origin		Destination		Trip Characteristics		
	θ (°W)	ϕ (°N)	θ (°W)	ϕ (°N)	value	distance (km)	time (days)
1	70	−13.5	200	−8.5	5,000	1.34×10^5	15.97
2	200	−8.5	210	1.5	5,000	2.40×10^6	27.08
3	210	1.5	320	11.5	5,000	2.14×10^6	23.84
4	320	11.5	240	10.5	5,000	1.29×10^6	19.44
5	240	10.5	120	18.5	5,000	1.54×10^6	17.36
6	120	18.5	90	4.5	5,000	3.01×10^6	27.20
7	90	4.5	330	10	5,000	3.26×10^6	18.06

Table 5.2. One-step heuristic's results of path planning among equal priority sites. Total travel time spent on this route is 148.96 days.

also with randomly generated research-values. The one-step heuristic's results in Table 5.6 demonstrate its greedy nature. Since most travel times in G' are similar, the larger relative differences between sites' values dominate the planning process. In Table 5.7, we show the two-step heuristic slightly offsetting this greediness with a longer term planning approach. It produces a slightly better path than the one-step heuristic. Finally, Table 5.8 shows the optimal path for this case.

Although the research-values associated with the seven interesting sites are completely different between this problem and the last, notice that the optimal paths are identical. The optimal path planning algorithm with $u_i = 0$ $\forall i \in N'$ contains an optimistic assumption—that the aerobot survives long enough to visit each site. Since we enumerate all paths, the one having the largest scientific value for any finite lifetime less than this maximum can be identified.

Trip	Origin		Destination		Trip Characteristics		
	θ (°W)	ϕ (°N)	θ (°W)	ϕ (°N)	value	distance (km)	time (days)
1	70	−13.5	200	−8.5	5,000	1.34×10^5	15.97
2	200	−8.5	240	10.5	5,000	2.43×10^6	30.09
3	240	10.5	90	4.5	5,000	1.51×10^6	23.96
4	90	4.5	320	11.5	5,000	3.25×10^6	17.71
5	320	11.5	330	10	5,000	1.39×10^6	21.41
6	330	10	120	18.5	5,000	1.16×10^6	22.80
7	120	18.5	210	1.5	5,000	3.14×10^6	29.86

Table 5.3. Two-step heuristic's results of path planning among equal priority sites. Total travel time spent on this route is 161.81 days. Notice that in this case, the two-step heuristic produces a longer path than the one-step heuristic. Although it most often produces shorter paths, there is no guarantee this will always occur.

Trip	Origin		Destination		Trip Characteristics		
	θ (°W)	ϕ (°N)	θ (°W)	ϕ (°N)	value	distance (km)	time (days)
1	70	−13.5	200	−8.5	5,000	1.34×10^5	15.97
2	200	−8.5	210	1.5	5,000	2.40×10^6	27.08
3	210	1.5	330	10	5,000	2.15×10^6	24.19
4	330	10	240	10.5	5,000	9.29×10^5	19.10
5	240	10.5	120	18.5	5,000	1.54×10^6	17.36
6	120	18.5	90	4.5	5,000	3.01×10^6	27.20
7	90	4.5	320	11.5	5,000	3.25×10^6	17.71

Table 5.4. Best path (with the shortest total travel time) for visiting several sites of equal priority. This is found by completely enumerating all distinct paths in G' and choosing the best. Total travel time is 148.61 days.

Site	θ (°W)	ϕ (°N)	Value
n_{ip}	70	−13.5	0
n_1	200	−8.5	4,125
n_2	210	1.5	1,456
n_3	90	4.5	3,324
n_4	320	11.5	702
n_5	330	10	3,451
n_6	240	10.5	1,763
n_7	120	18.5	1,162

Table 5.5. In this problem, sites have randomly generated research-value. Therefore, the largest cost-to-value ratio depends on both travel times and research-values. We number sites as in Table 5.1.

Trip	Origin		Destination		Trip Characteristics		
	θ (°W)	ϕ (°N)	θ (°W)	ϕ (°N)	value	distance (km)	time (days)
1	70	−13.5	200	−8.5	4,125	1.34×10^5	15.97
2	200	−8.5	330	10	3,451	2.52×10^6	29.63
3	330	10	90	4.5	3,324	1.14×10^6	28.70
4	90	4.5	240	10.5	1,763	3.54×10^6	23.84
5	240	10.5	120	18.5	1,162	1.54×10^6	17.36
6	120	18.5	210	1.5	1,456	3.14×10^6	29.86
7	210	1.5	320	11.5	702	2.14×10^6	23.84

Table 5.6. One-step heuristic's results of path planning among varied priority sites. Total travel time spent on this route is 169.21 days.

Trip	Origin		Destination		Trip Characteristics		
	θ (°W)	ϕ (°N)	θ (°W)	ϕ (°N)	value	distance (km)	time (days)
1	70	−13.5	200	−8.5	4,125	1.34×10^5	15.97
2	200	−8.5	90	4.5	3,324	2.65×10^6	32.18
3	90	4.5	330	10	3,451	3.26×10^6	18.06
4	330	10	240	10.5	1,763	9.29×10^5	19.10
5	240	10.5	120	18.5	1,162	1.54×10^6	17.36
6	120	18.5	210	1.5	1,456	3.14×10^6	29.86
7	210	1.5	320	11.5	702	2.14×10^6	23.84

Table 5.7. Two-step heuristic's results of path planning among varied priority sites. Total travel time spent on this route is 156.37 days—a slightly shorter path than produced by the one-step heuristic.

Trip	Origin		Destination		Trip Characteristics		
	θ (°W)	ϕ (°N)	θ (°W)	ϕ (°N)	value	distance (km)	time (days)
1	70	−13.5	200	−8.5	4,125	1.34×10^5	15.97
2	200	−8.5	210	1.5	1,456	2.40×10^6	27.08
3	210	1.5	330	10	3,451	2.15×10^6	24.19
4	330	10	240	10.5	1,763	9.29×10^5	19.10
5	240	10.5	120	18.5	1,162	1.54×10^6	17.36
6	120	18.5	90	4.5	3,324	3.01×10^6	27.20
7	90	4.5	320	11.5	702	3.25×10^6	17.71

Table 5.8. Best path (with the shortest total travel time) for visiting several sites with varied priority. Found by completely enumerating all distinct paths in G' and choosing the best. Total travel time is 148.61 days.

E. AN ELEVEN SITE MISSION

As mentioned earlier, any world explored by an aerobot is likely to have many interesting sites. Here we solve an eleven site mission with randomly generated research-values (Table 5.9). We again use $u_i = 0 \quad \forall\, i \in N'$. Because of the exponential nature of complete enumeration, problems with more interesting sites than this should only be solved heuristically.

The one-step heuristic's solution (Table 5.10) seeks higher priority sites early in the mission. Table 5.11 shows the two-step heuristic's solution which pursues a similar but farther-sighted strategy, resulting in a 10% better solution. The optimal solution in Table 5.12 again assumes a sufficient lifetime to visit all sites and clearly pays little heed to sites' research-values, focusing instead on total travel time. With all paths enumerated, the one with the largest scientific value for any finite lifetime less than this maximum can be identified. Also note that the optimal solution is only 10% better than that of the two-step heuristic.

Site	$\theta\,(°\mathrm{W})$	$\phi\,(°\mathrm{N})$	Value
n_{ip}	70	−13.5	0
n_1	170	7	6413
n_2	130	24.5	6053
n_3	50	20	5794
n_4	300	15.5	4970
n_5	270	15	4439
n_6	70	20	2548
n_7	210	−20	2385
n_8	180	19.5	1607
n_9	90	16.5	996
n_{10}	240	−20	853
n_{11}	330	−22.5	753

Table 5.9. A larger problem with eleven interesting sites and randomly generated research-values.

F. PROTOTYPE VFR MISSION

As mentioned earlier, scientists have started to choose and prioritize the interesting sites at Venus. Specifically, planetary geologists are most interested in tessera terrain (thought to be some of the oldest sections of the Venusian crust) and the boundaries between plains and tessera terrain. The next priority is terrain with farra or steep-sided

Trip	Origin		Destination		Trip Characteristics		
	$\theta\,(^\circ\mathrm{W})$	$\phi\,(^\circ\mathrm{N})$	$\theta\,(^\circ\mathrm{W})$	$\phi\,(^\circ\mathrm{N})$	value	distance (km)	time (days)
1	70	−13.5	170	7	6413	4.82×10^{5}	25.00
2	170	7	50	20	5794	3.63×10^{6}	17.13
3	50	20	130	24.5	6053	5.10×10^{6}	20.72
4	130	24.5	300	15.5	4970	4.21×10^{6}	24.77
5	300	15.5	270	15	4439	1.29×10^{6}	20.02
6	270	15	70	20	2548	1.80×10^{6}	23.03
7	70	20	180	19.5	1607	4.81×10^{6}	22.45
8	180	19.5	210	−20	2385	3.79×10^{6}	35.53
9	210	−20	240	−20	853	2.70×10^{6}	20.72
10	240	−20	330	−22.5	753	2.43×10^{6}	21.41
11	330	−22.5	90	16.5	996	1.11×10^{6}	37.85

Table 5.10. One-step heuristic's results of path planning for the data in Table 5.9. Note that sites with higher research-value tend to be visited earlier, but that this is not a firm rule. Sometimes a site's proximity makes it very appealing even though it has little research-value. Total travel time spent on this route is 268.63 days.

Trip	Origin		Destination		Trip Characteristics		
	$\theta\,(^\circ\mathrm{W})$	$\phi\,(^\circ\mathrm{N})$	$\theta\,(^\circ\mathrm{W})$	$\phi\,(^\circ\mathrm{N})$	value	distance (km)	time (days)
1	70	−13.5	170	7	6413	4.82×10^{5}	25.00
2	170	7	130	24.5	6053	3.70×10^{6}	17.94
3	130	24.5	50	20	5794	3.97×10^{6}	18.87
4	50	20	300	15.5	4970	4.93×10^{6}	18.75
5	300	15.5	270	15	4439	1.29×10^{6}	20.02
6	270	15	70	20	2548	1.80×10^{6}	23.03
7	70	20	180	19.5	1607	4.81×10^{6}	22.45
8	180	19.5	90	16.5	996	3.30×10^{6}	18.98
9	90	16.5	330	−22.5	753	4.63×10^{6}	32.29
10	330	−22.5	210	−20	2385	4.88×10^{5}	17.94
11	210	−20	240	−20	853	2.70×10^{6}	20.72

Table 5.11. Two-step heuristic's results of path planning in a larger problem. Total travel time spent on this route is 236.00 days. This is about 10% shorter than the path produced by the one-step heuristic.

Trip	Origin		Destination		Trip Characteristics		
	θ (°W)	ϕ (°N)	θ (°W)	ϕ (°N)	value	distance (km)	time (days)
1	70	−13.5	240	−20	853	1.69×10^5	15.05
2	240	−20	330	−22.5	753	2.43×10^6	21.41
3	330	−22.5	210	−20	2385	4.88×10^5	17.94
4	210	−20	170	7	6413	3.02×10^6	35.53
5	170	7	90	16.5	996	3.67×10^6	18.29
6	90	16.5	270	15	4439	4.20×10^6	17.13
7	270	15	130	24.5	6053	1.50×10^6	16.32
8	130	24.5	70	20	2548	3.99×10^6	19.33
9	70	20	300	15.5	4970	4.58×10^6	18.52
10	300	15.5	180	19.5	1607	1.19×10^6	17.48
11	180	19.5	50	20	5794	3.25×10^6	17.36

Table 5.12. Best path (with the shortest total travel time) for visiting several sites in the larger problem. Found by completely enumerating all distinct paths in G' and choosing the best. Total travel time is 214.35 days, about 20% better than the path produced by the one-step heuristic.

domes. These are pancake-like structures thought to be associated with vulcanism, but nothing like them has been observed anywhere else in the solar system. There are three such domes in Tinatin Planitia, a low-lying plain near Guinevere Planitia (Figures 5.1 and 5.15). They are most likely caused by upwellings of magma from deep within the planet's mantle. Geologists are also interested in coronae. Artemis Corona (Figures 5.2 and 5.15) is the largest corona on Venus and is thought to be a location where subduction (like that on Earth) occurs. Although still very interesting to geologists, large regions that are highly reflective to radar like Thetis Regio (Figure 5.3), Ovda Regio, and Atla Regio, along with mountains like Ozza Mons, Maat Mons, Gula Mons, and Sif Mons are of lesser importance than the other terrain types [Head *et al.* 1996].

As a final example of this thesis' results, we use a subset of 28 such sites for planning a prototypical mission for VFR. Table 5.13 shows these sites. Most also appear in Figure 5.15. Table 5.14 shows the route planned by the one-step heuristic and Table 5.15 shows that of the two-step heuristic. These two path lengths differ only by about 2%.

G. PATH PROFILES

The tables in this chapter succinctly summarize an entire aerobot mission from atmosphere insertion to final destination, however, there is much detail that they cannot represent. The atmosphere of Venus is very complex and since an aerobot is wind-born while voyaging, the paths between any origin and destination are similarly complex—they

follow the wind patterns. Besides origin and destination, information about these paths is completely absent from the tables profiling an entire mission. These *paths* are interesting in their own light, however. Studying them reveals a great deal about atmospheric characteristics and may help a planner to better choose and prioritize exploration sites.

Although the GCM in this thesis is only a simplified model and lacks much detail, aerobot paths through it are still surprisingly complex and offer a great deal of insight. In this section, we present a sampling of the paths between sites for the VFR mission just planned. Although we do not show all 25 trips required to visit the feasible sites, Figures 5.4, 5.5, 5.6, 5.7, 5.8, and 5.9 show the first six trips after insertion that VFR takes to explore the planet. We show other routes in Figures 5.10, 5.11, and 5.12 because they demonstrate some unusual and interesting paths through the GCM. Refer to Figure 4.1 to place these paths in context with the remaining nodes of the GCM.

Site	Name of Geographic Feature	θ (°W)	ϕ (°N)	Value
n_{ip}		70	-13.5	0
n_1	Flosshilde Farra	80	10	7500
n_2	Carmenta Farra	350	12	7000
n_3	Liban Farra	10	-25	7000
n_4	Parga Chasma and Corona	110	15	7000
n_5	Artemis Chasma and Corona	220	-27	7000
n_6	Oshun Farra	340	5	6800
n_7	Seoritsu Farra	350	-30	6500
n_8	Diana Chasma	200	-10	6000
n_9	Dali Chasma	190	-20	6000
n_{10}	Ganis Chasma	170	25	6000
n_{11}	Rusalka Planitia	180	0	5500
n_{12}	Ozza Mons	160	4	5000
n_{13}	Maat Mons	170	1	5000
n_{14}	Crest of Atla Regio	160	0	5000
n_{15}	Crest of Ovda Regio	260	-6.5	5000
n_{16}	Phoebe Regio	80	-6.5	5000
n_{17}	Thetis Regio	230	-10	4000
n_{18}	Ulfrun Regio	140	20	4000
n_{19}	Asteria Regio	90	20	4000
n_{20}	Beta Regio	70	25	3000
n_{21}	Hyndla Regio	60	20	3000
n_{22}	Gula Mons	0	22	1000
n_{23}	Sif Mons	10	25	1000
n_{24}	Theia Mons	80	25	1000
n_{25}	Center of Alpha Regio	0	-25	1000
n_{26}	Sappho Patera	340	13	1000
n_{27}	Theodora Patera	70	20	500
n_{28}	Eve (large ovoid-shaped feature)	0	-30	500

Table 5.13. A more realistic problem containing 28 interesting sites with their geographic names and features. Research-values are based on rough measures of importance as indicated by Head *et al.* [1996].

Trip	Origin		Destination		Trip Characteristics		
	$\theta\,(°\mathrm{W})$	$\phi\,(°\mathrm{N})$	$\theta\,(°\mathrm{W})$	$\phi\,(°\mathrm{N})$	value	distance (km)	time (days)
1	70	−13.5	10	−25	7000	2.90×10^{5}	16.78
2	10	−25	190	−20	6000	1.99×10^{6}	23.96
3	190	−20	200	−10	6000	5.61×10^{6}	22.45
4	200	−10	80	−6.5	5000	5.86×10^{6}	19.10
5	80	−6.5	260	−6.5	5000	1.69×10^{6}	17.36
6	260	−6.5	80	10	7500	3.29×10^{6}	25.93
7	80	10	350	12	7000	2.56×10^{6}	18.87
8	350	12	110	15	7000	3.05×10^{6}	22.92
9	110	15	170	25	6000	4.49×10^{6}	20.02
10	170	25	340	5	6800	5.01×10^{6}	31.37
11	340	5	160	4	5000	9.10×10^{5}	17.48
12	160	4	90	20	4000	3.68×10^{6}	17.94
13	90	20	140	20	4000	3.34×10^{6}	21.06
14	140	20	180	0	5500	8.52×10^{5}	29.86
15	180	0	170	1	5000	4.15×10^{6}	21.41
16	170	1	160	0	5000	3.38×10^{6}	25.69
17	160	0	70	25	3000	6.22×10^{6}	16.90
18	70	25	60	20	3000	2.91×10^{6}	20.25
19	60	20	230	−10	4000	2.77×10^{6}	34.26
20	230	−10	0	−25	1000	1.75×10^{6}	21.18
21	0	−25	10	25	1000	1.07×10^{6}	35.76
22	10	25	0	22	1000	2.09×10^{6}	19.91
23	0	22	80	25	1000	2.50×10^{6}	20.72
24	80	25	340	13	1000	1.74×10^{6}	26.04
25	340	13	70	20	500	3.37×10^{6}	21.53

Table 5.14. One-step heuristic's results of path planning for a realistic problem. Total travel time spent on this route is 568.75 days.

Trip	Origin		Destination		Trip Characteristics		
	θ (°W)	ϕ (°N)	θ (°W)	ϕ (°N)	value	distance (km)	time (days)
1	70	−13.5	200	−10	6000	1.33×10^5	15.63
2	200	−10	80	−6.5	5000	5.86×10^6	19.10
3	80	−6.5	10	−25	7000	1.79×10^6	17.25
4	10	−25	180	0	5500	2.01×10^6	32.87
5	180	0	80	10	7500	4.05×10^6	18.40
6	80	10	110	15	7000	2.68×10^6	20.95
7	110	15	350	12	7000	4.33×10^6	18.75
8	350	12	170	25	6000	3.08×10^6	22.22
9	170	25	160	4	5000	4.84×10^6	30.21
10	160	4	340	5	6800	3.57×10^6	17.25
11	340	5	170	1	5000	9.21×10^5	23.15
12	170	1	260	−6.5	5000	3.48×10^6	22.92
13	260	−6.5	160	0	5000	3.00×10^6	24.31
14	160	0	190	−20	6000	6.71×10^6	28.24
15	190	−20	230	−10	4000	5.63×10^6	23.03
16	230	−10	340	13	1000	1.77×10^6	29.51
17	340	13	90	20	4000	3.38×10^6	21.88
18	90	20	140	20	4000	3.34×10^6	21.06
19	140	20	60	20	3000	7.20×10^5	18.40
20	60	20	70	25	3000	2.58×10^6	19.33
21	70	25	80	25	1000	2.92×10^6	19.56
22	80	25	10	25	1000	1.76×10^6	18.06
23	10	25	0	22	1000	2.09×10^6	19.91
24	0	22	70	20	500	2.50×10^6	21.64
25	70	20	0	−25	1000	1.79×10^6	33.56

Table 5.15. Two-step heuristic's results of path planning for a realistic problem. Total travel time spent on this route is 557.18 days. This is only 2% shorter than the path found by the one-step heuristic.
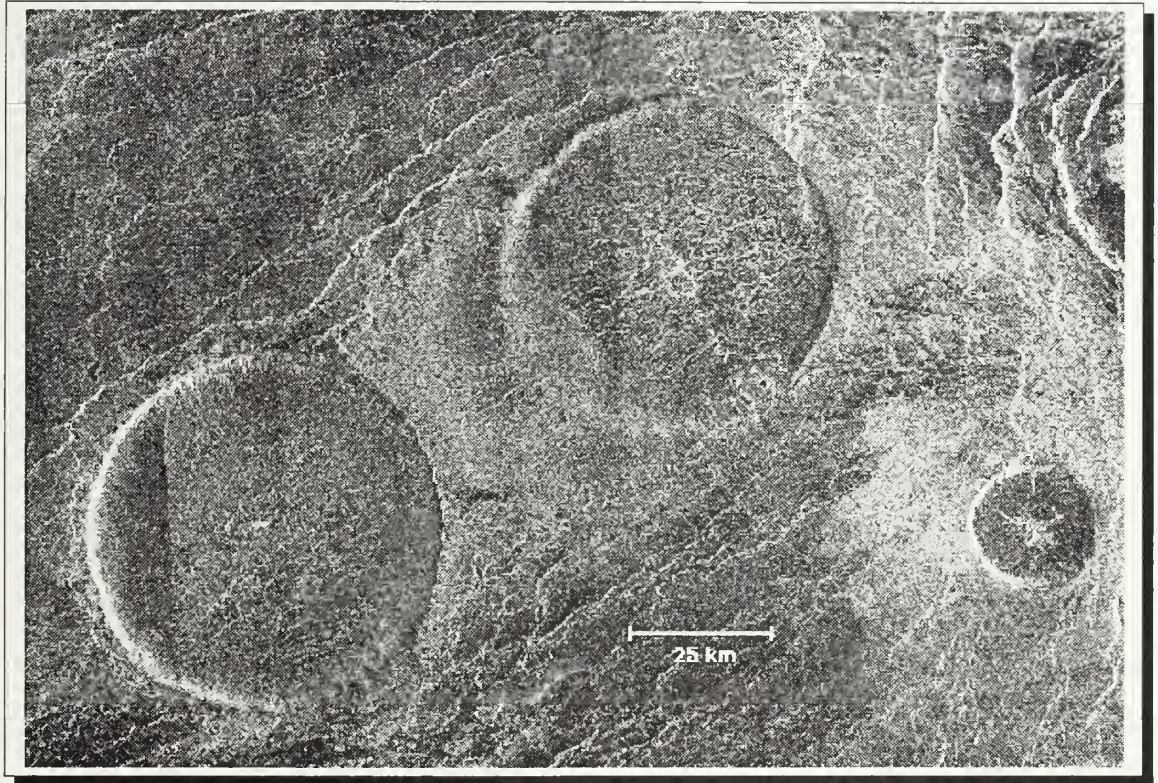
Figure 5.1. Three steep-sided domes in Tinatin Planitia located at 12°N, 8°E with approximate radii of 31 km, 29 km, and 10.3 km. Magellan image from C1-MIDR at 15°N, 9°E. Illumination is from the left. Geological formations like these are unique to Venus and planetary geologists associate them with the buoyant ascent of magma from deep within the Venusian mantle. See Figure 5.15 for location of this site relative to other interesting geological features on Venus. Source: http://www-geodyn.mit.edu/tube.html.
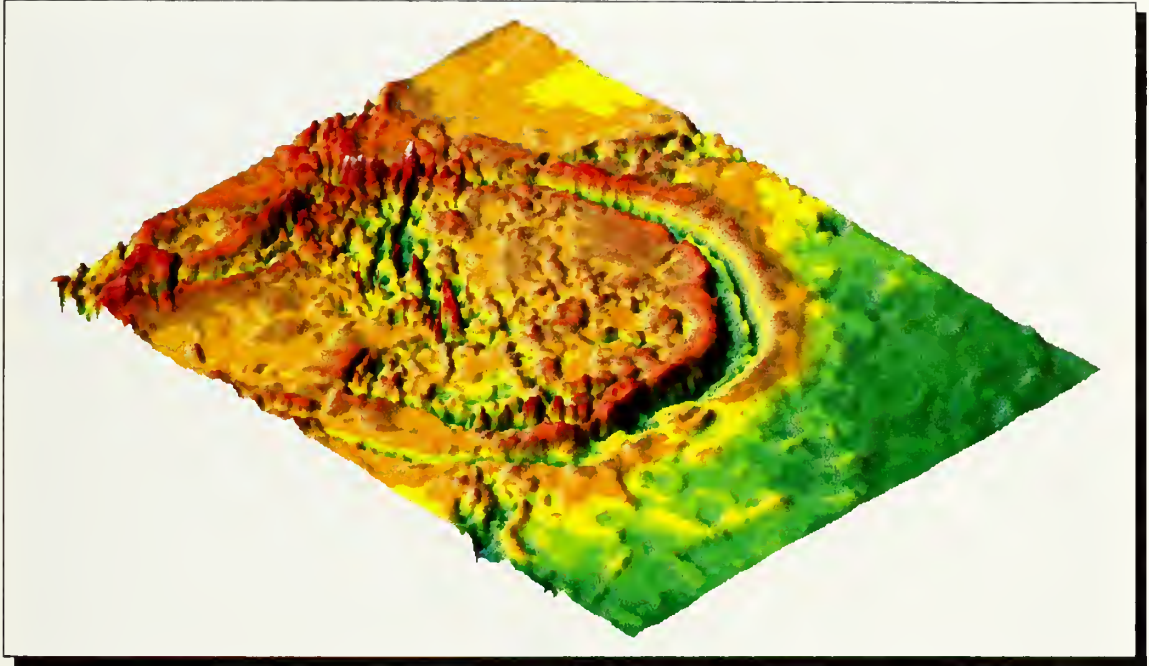
Figure 5.2. The largest corona on Venus, Artemis was initially recognized as a chasma based on Pioneer Venus topography data (Figure 5.15) which revealed a deep, curving depression. More detailed topography from Magellan shows a nearly circular trench (Artemis Chasma) that surrounds the corona with a diameter of over 2,000 km (1,250 miles). The corona rim rises as much as 6,000 m (20,000 ft) above the bottom of this trench, and the interior is a plateau standing 2,000 m (6,500 ft) above the surrounding plains. Based on the similarity of the shape of the trench to the shapes of subduction zones on Earth and on the presence of positive gravity and geoid height anomalies over the plateau, Artemis Corona has been identified as a potential location of subduction on Venus. Source: http://www.ess.ucla.edu/hypermap/coronae/artemis.html.
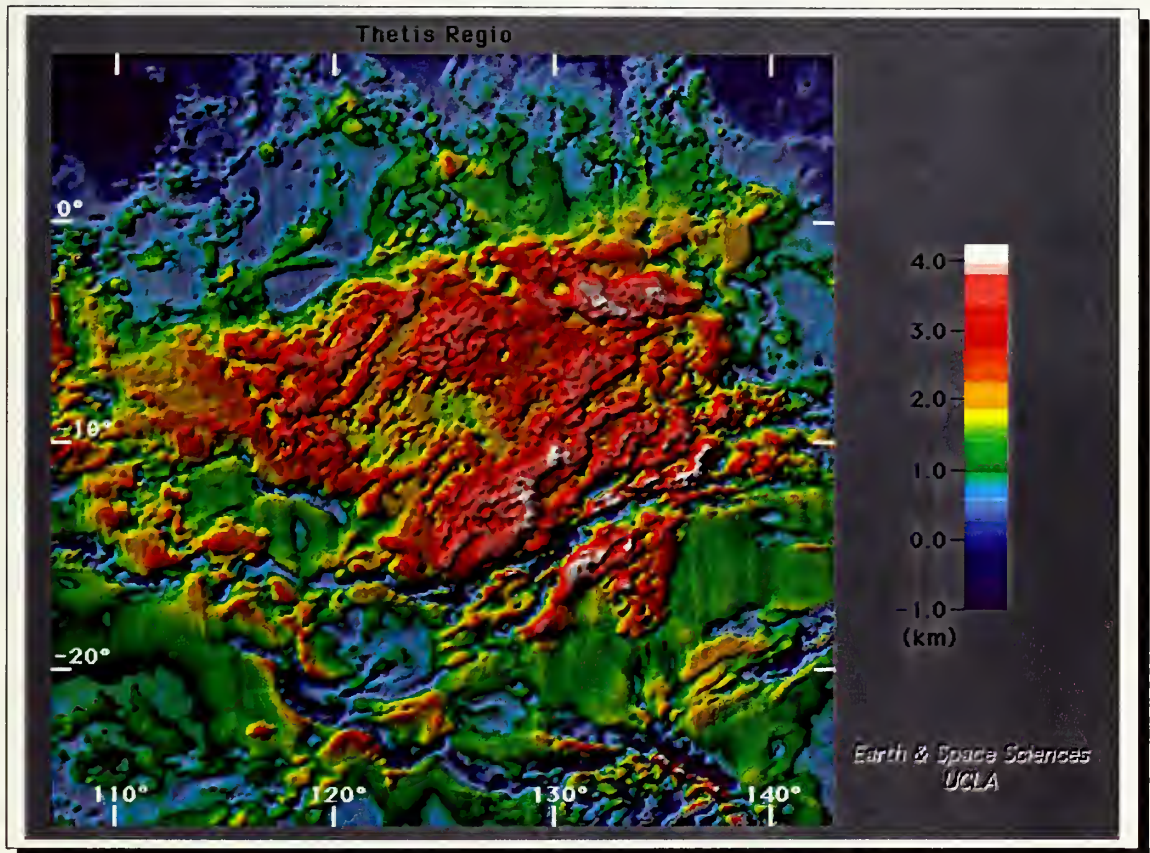
Figure 5.3. Regio are large areas marked by reflectivity or color distinctions from adjacent areas. Here we show Thetis Regio with color contours marking elevation of terrain relative to the mean planetary radius. Figure 5.15 shows Thetis Regio between Ovda Regio and Atla Regio in Aphrodite Terra. Source: `http://www.ess.ucla.edu/hypermap/highlands/thetis.html`.
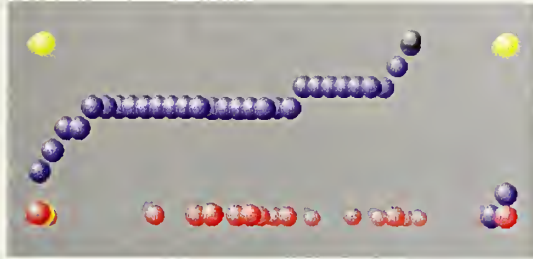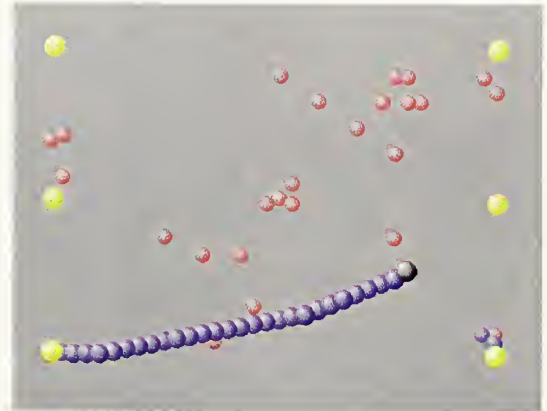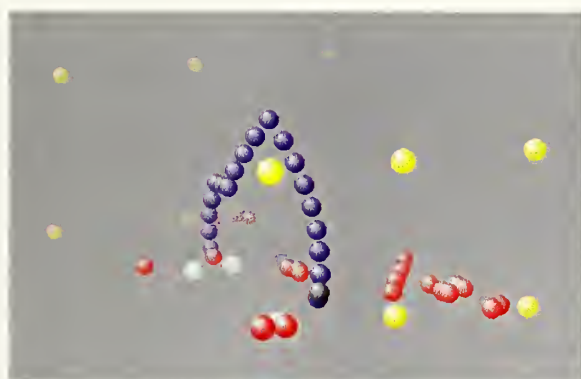
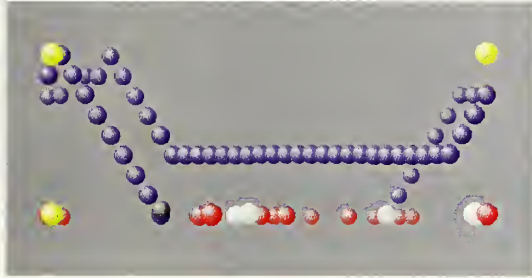(a) Side view looking northward. Westward is to the left.
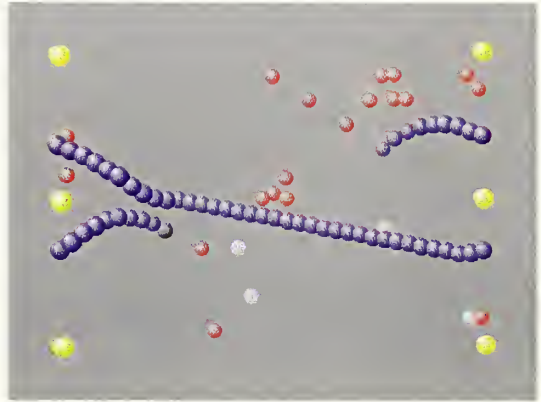

(b) Top view looking downward. Westward is to the left.
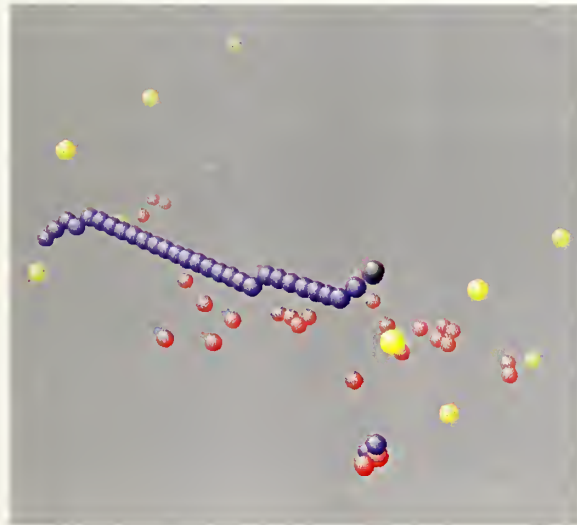
(c) A three-dimensional perspective looking downward and to the northwest.

Figure 5.4. The route VFR follows from the atmosphere insertion point, n_{ip} to Liban Farra, a group of steep-sided domes near Alpha Regio. The colored spheres represent nodes in the GCM (see Figure 4.1 for a sketch of all nodes). Red spheres are unexplored interesting sites on the planet's surface, yellow spheres mark the corners and equator of the GCM, and blue spheres highlight the path from the origin of a trip (marked with a grey sphere) to its destination.
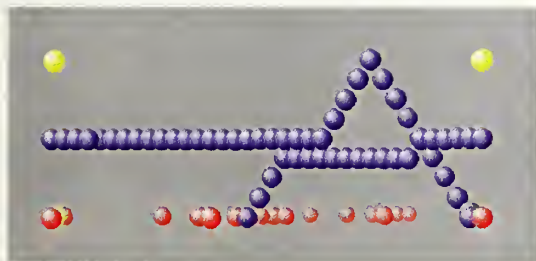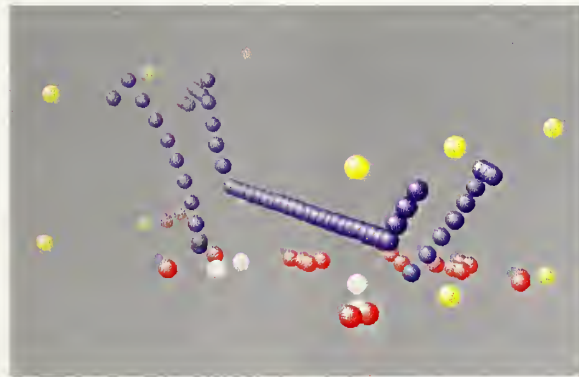
(a) Side view looking northward. Westward is to the left.
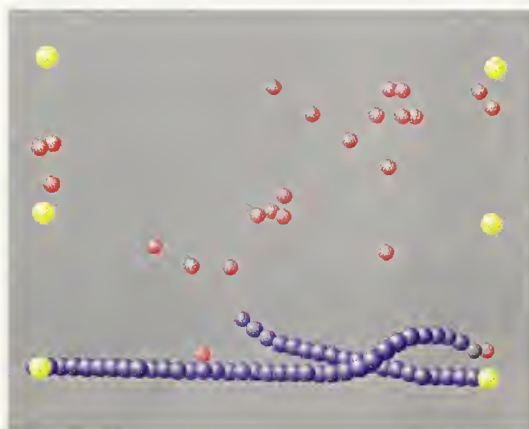
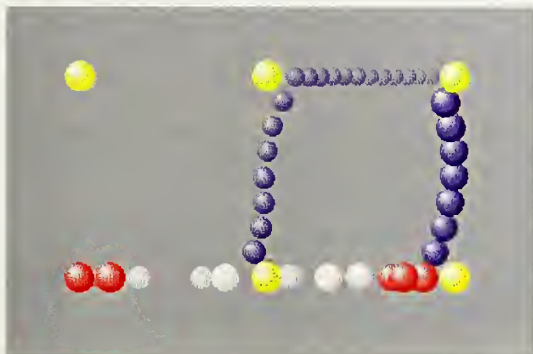(b) Top view looking downward. Westward is to the left.
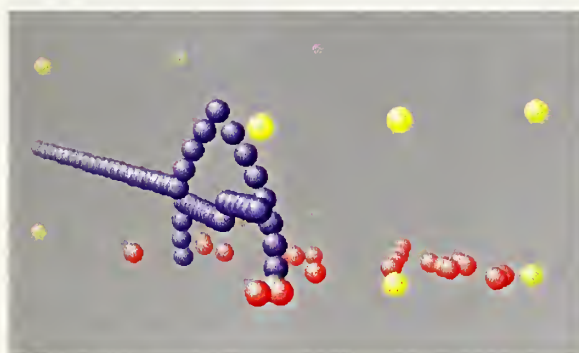
(c) A three-dimensional perspective looking downward and to the northwest.

Figure 5.5. The route VFR follows from Liban Farra (grey sphere) to Dali Chasma, a prominent rift in Aphrodite Terra between Thetis Regio and Atla Regio. See Figure 5.15 for locations of these sites relative to other planetary features.
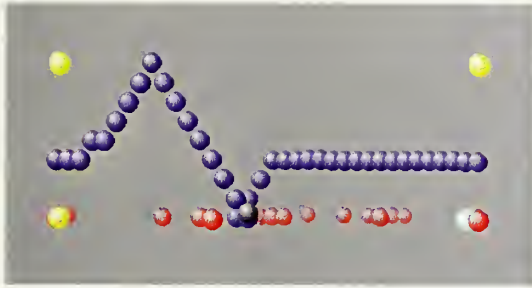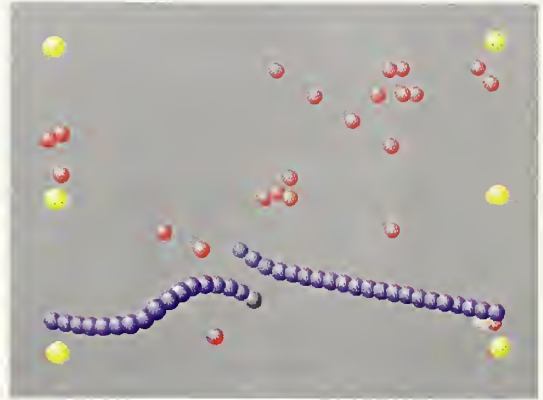
51

(a) Side view looking northward. Westward is to the left.

(b) Top view looking downward. Westward is to the left.
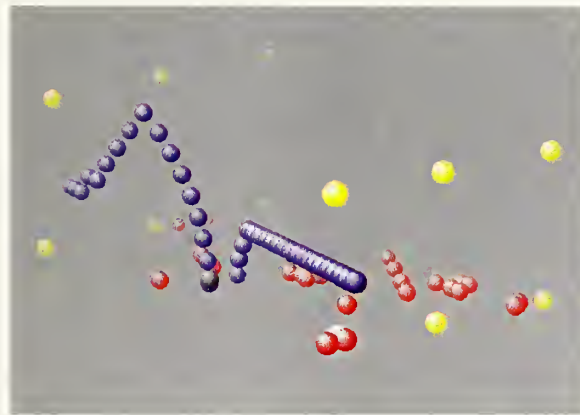
(c) A three-dimensional perspective looking downward and to the northwest.

Figure 5.6. The route VFR follows from Dali Chasma (grey sphere) to Diana Chasma, another prominent rift in Aphrodite Terra near Dali Chasma. The white sphere in the lower Southeastern corner of the GCM is Liban Farra. It is white indicating that it has already been visited by VFR. The red spheres are interesting sites that remain on VFR's itinerary.
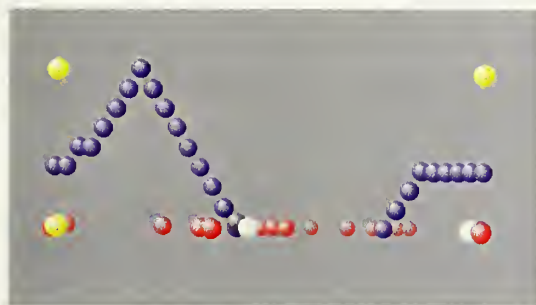
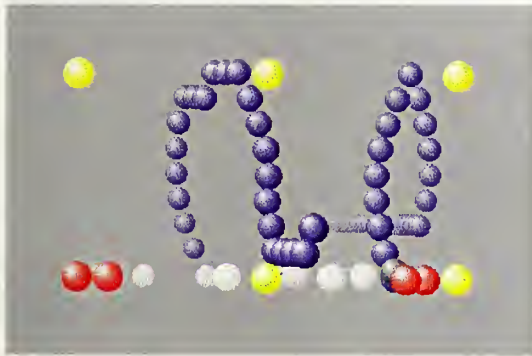(a) Side view looking northward. Westward is to the left.
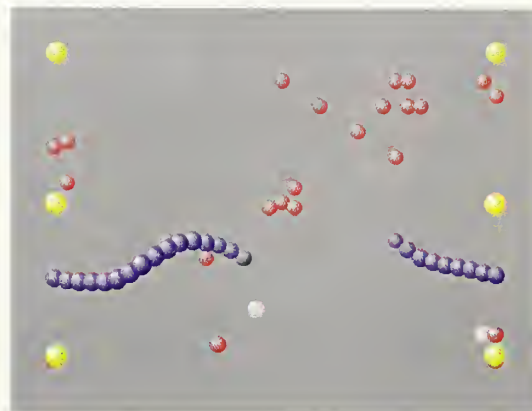
(b) Top view looking downward. Westward is to the left.
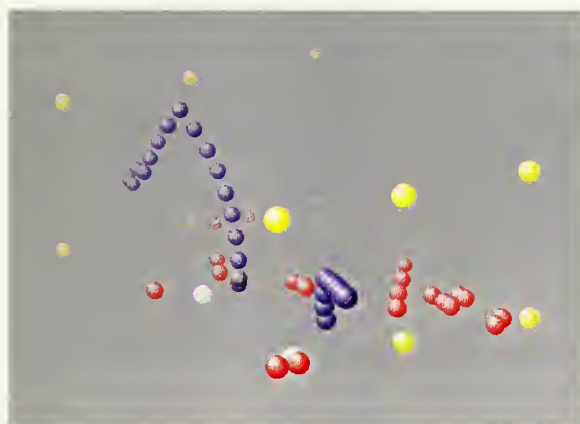
(c) A three-dimensional perspective looking downward and to the northwest.

Figure 5.7. The route VFR follows from Diana Chasma (grey sphere) to the crest of Phoebe Regio, located between Asteria Regio and Themis Regio. Now both Liban Farra and Dali Chasma have been visited as indicated by their white color.
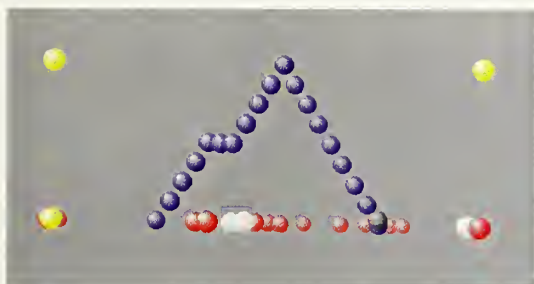
(a) Side view looking northward. Westward is to the left.
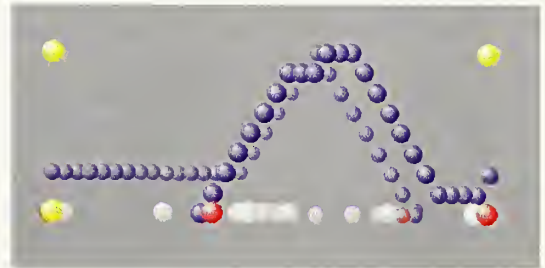

(b) Top view looking downward. Westward is to the left.

(c) A three-dimensional perspective looking downward and to the northwest.

Figure 5.8. The route VFR follows from Phoebe Regio (grey sphere) to the crest of Ovda Regio at the far Western edge of Aphrodite Terra. Although this path shows VFR returning to the planetary surface immediately after reaching its EA, the time spent on this trip includes a four day trip around the planet (not shown) while at EA to permit adequate cooling time before returning to the hot surface.

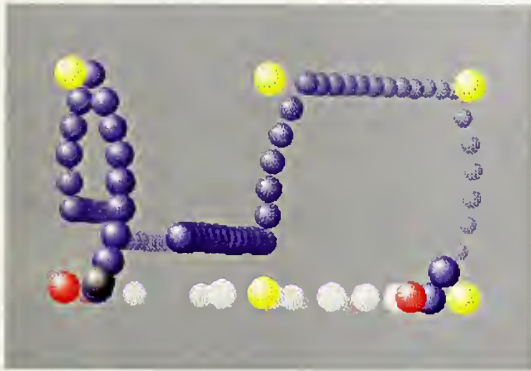(a) Side view looking northward. Westward is to the left.

(b) Top view looking downward. Westward is to the left.

(c) A three-dimensional perspective looking downward and to the northwest.

Figure 5.9. The route VFR follows from Ovda Regio (grey sphere) to Flosshilde Farra, another group of steep-sided domes situated in a low-lying plain midway between Rhea Mons and Phoebe Regio.

(a) Forward view looking directly downwind or westward. Southward is to the left.

(b) Side view looking northward. Westward is to the left.
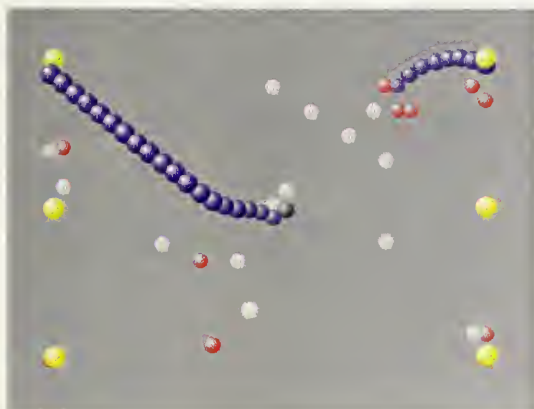
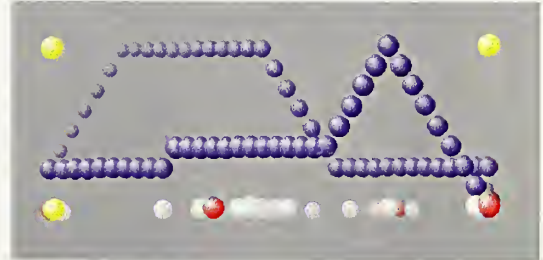(c) Top view looking downward. Westward is to the left.
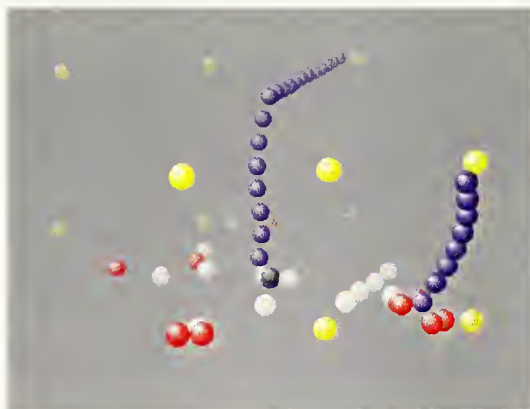
(d) A three-dimensional perspective looking downward and to the northwest.

Figure 5.10. The route VFR follows from Atla Regio (grey sphere) near the Eastern edge of Aphrodite Terra to Beta Regio near Rhea Mons and Theia Mons.

(a) Forward view looking directly downwind or westward. Southward is to the left.

(b) Side view looking northward. Westward is to the left.
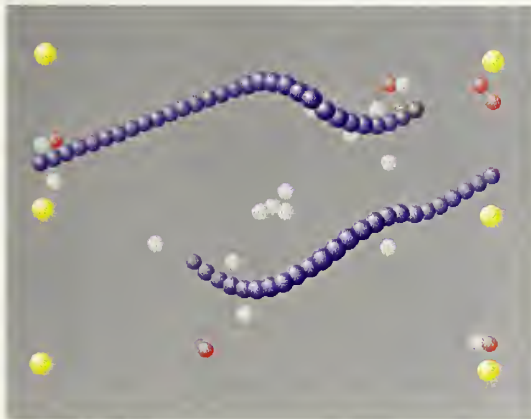
(c) Top view looking downward. Westward is to the left.
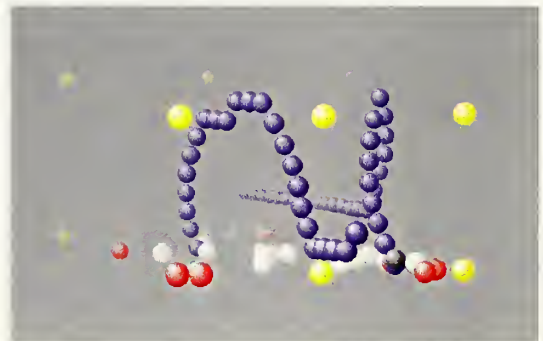
(d) A three-dimensional perspective looking downward and to the northwest.

Figure 5.11. The route VFR follows from Hyndla Regio (grey sphere) just East of Theodora Patera to Thetis Regio. Figure 5.15 shows Thetis Regio between Ovda Regio and Atla Regio in Aphrodite Terra. Figure 5.3 shows a more detailed image of Thetis Regio.

(a) Forward view looking directly downwind or westward. Southward is to the left.

(b) Side view looking northward. Westward is to the left.
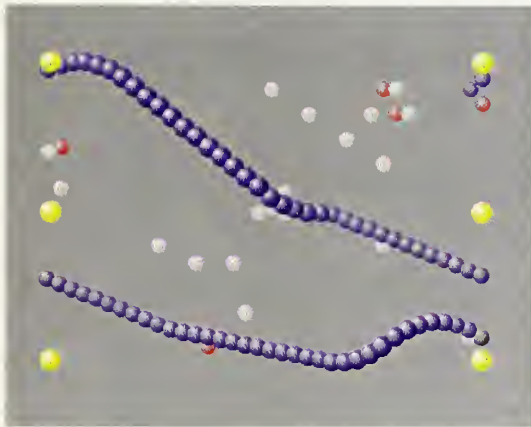
(c) Top view looking downward. Westward is to the left.
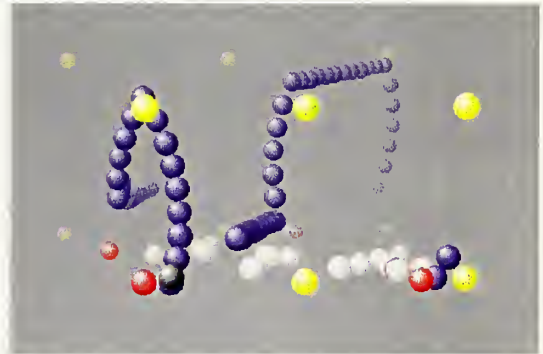
(d) A three-dimensional perspective looking downward and to the northwest.

Figure 5.12. The route VFR follows from Alpha Regio (grey sphere) between Lavinia Planitia and Aino Planitia to Sif Mons at the Western edge of Eistla Regio. The equator-crossing portion of the trip shown here and in Figures 5.9 and 5.11 occurs at a low altitude because the GCM includes only a single Hadley Cell. Therefore, meridional winds that are equator-ward only occur in the bottom half of the GCM.
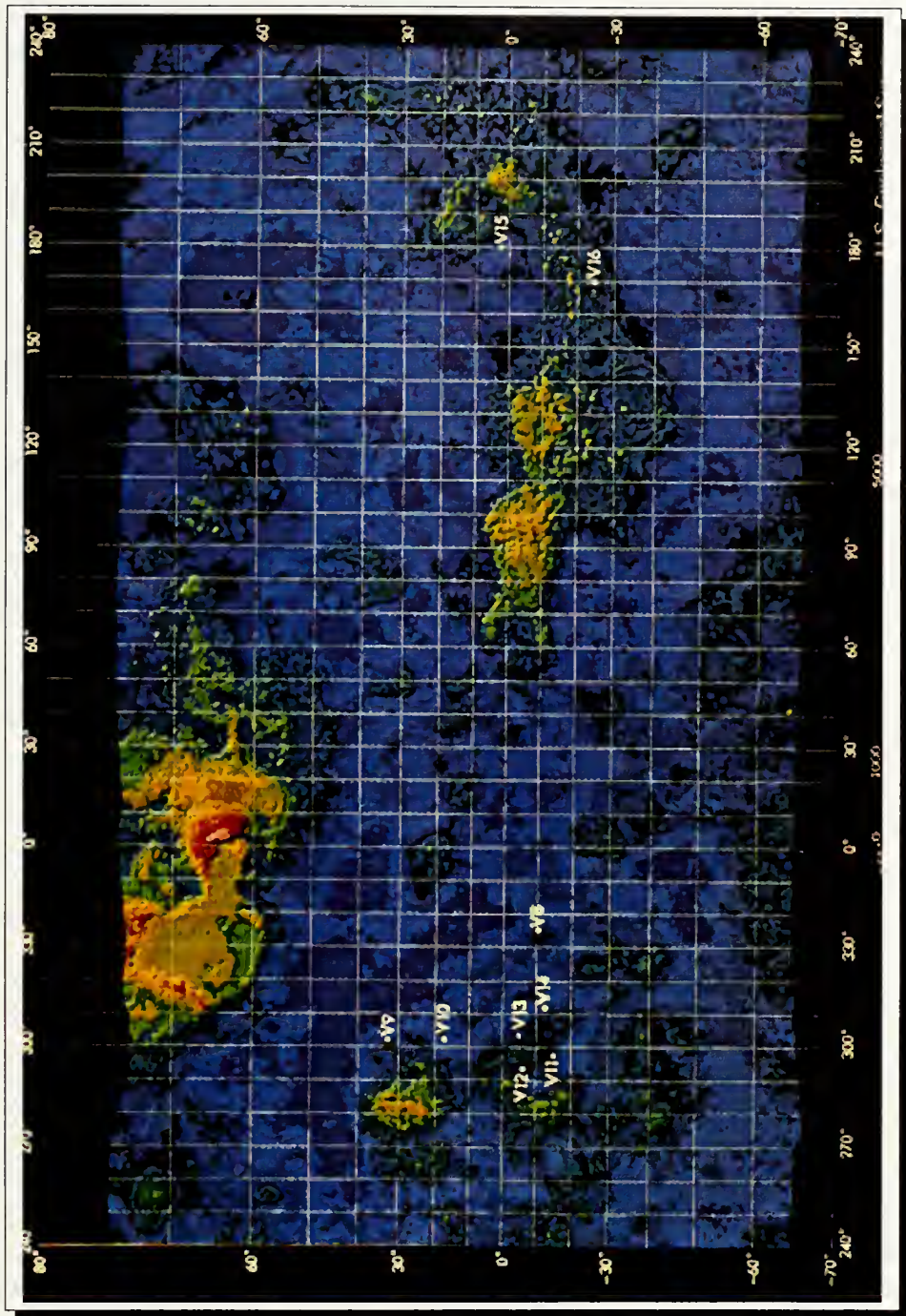
Figure 5.13. Topography of Venus according to Pioneer Venus Orbiter. Color contours show surface elevation with dark blue indicating lowest and bright red indicating highest. Entry sites of several Russian Venera probes are shown. Figure 5.14 shows a different perspective of some of the same locations, as well as entry sites of several US exploratory probes. The Mercator projection exaggerates the areas of features at high latitudes. Source: [Hunten *et al.* 1983].
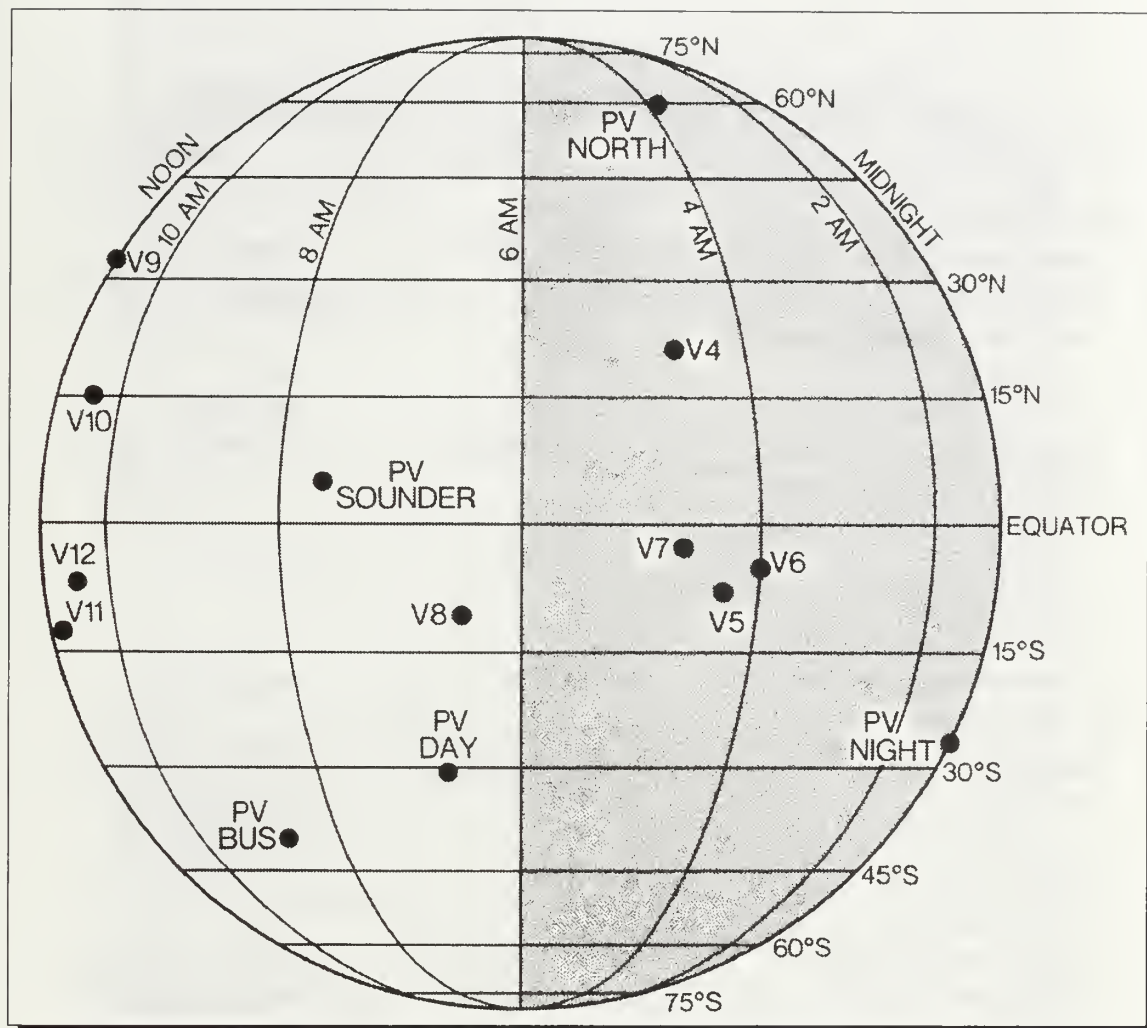
Figure 5.14. The entry locations of the Pioneer Venus (PV) and Venera (V) probes. All the probes penetrated the deep atmosphere except the PV bus which burned up at 110 km. These sites are all in the equatorial region between ~30°S and ~30°N except for the PV North probe which entered at 60°N. Almost all the probes have entered between local midnight (the antisolar meridian) and local noon (the subsolar meridian). The V11 and V12 probes landed shortly after noon. Also see Figure 5.13 for locations of the probes relative to planetary features. Source: [Hunten *et al.* 1983].
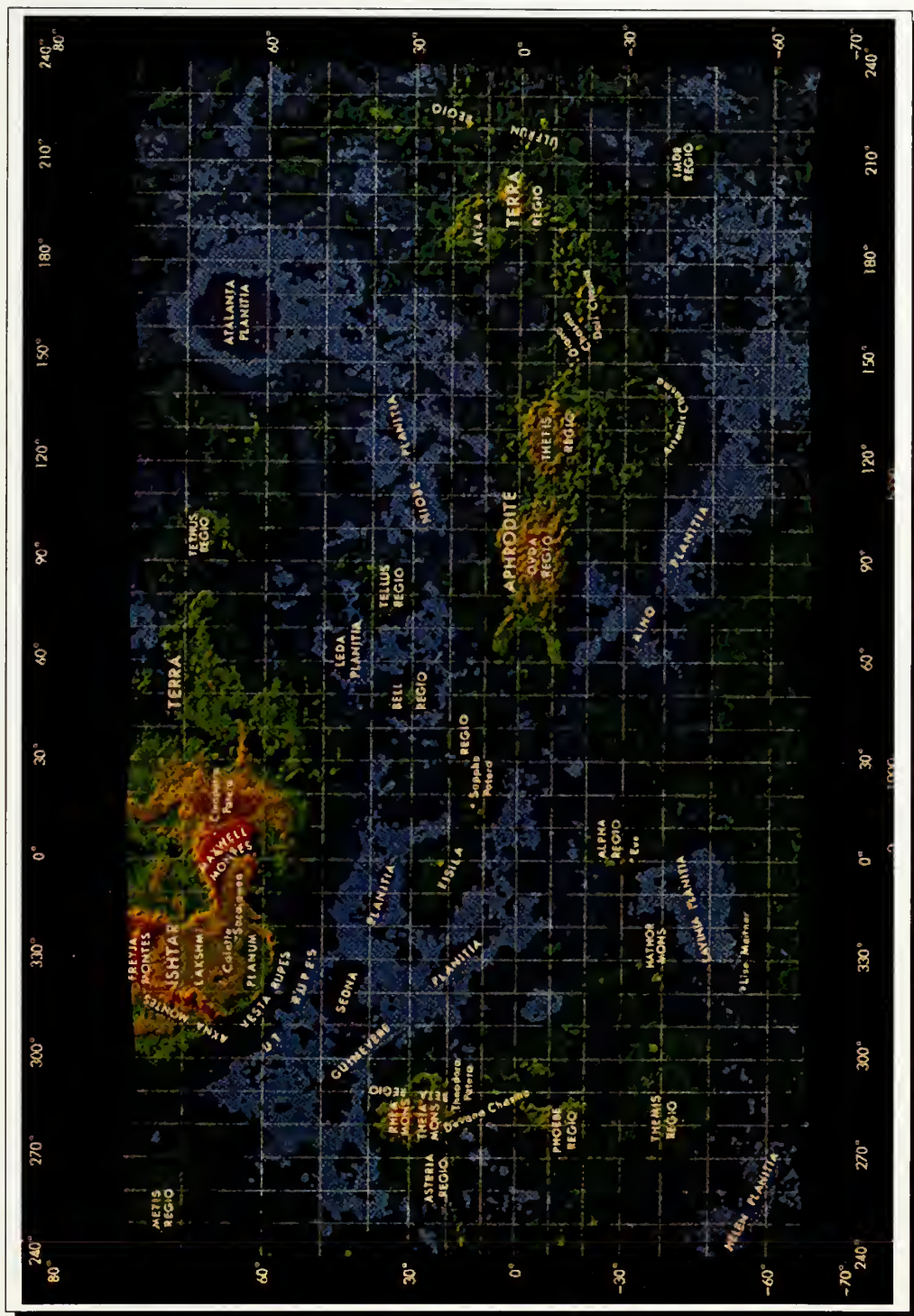
Figure 5.15. Topography of Venus according to Pioneer Venus Orbiter. Color contours show surface elevation with dark blue indicating lowest and bright red indicating highest. The Mercator projection exaggerates the areas of features at high latitudes. Source: [Hunten *et al.* 1983].

VI. CONCLUSION

Planetary exploration pushes the boundaries of human knowledge. A passionate interest in the exploration of our universe—be that the neighboring countries, the continents across the ocean, or the planets of our solar system and realms beyond—has always been a strong characteristic of our species. Learning "...why the world wags and what wags it..." [White 1958] is a deep-seated desire in humans and we reap many great benefits from this curiosity.

The things we learn in exploring nature continuously raise our standard of living and often do so in completely unanticipated ways. There are many obvious and practical benefits that fully justify exploring neighboring worlds—we find important clues to the past and potential future of *our* planet in doing so.

For example, concern about the "greenhouse effect" on Earth came about largely as a result of the discovery that the atmosphere on Venus is loaded with carbon dioxide and that it is much hotter than it should be given its proximity to the Sun. We now understand enough about the Venusian atmosphere to see the results of a runaway greenhouse effect and realize that some of the same processes are occurring on Earth. With this knowledge, we may avoid initiating a similar problem on our world as we slowly change its global environment by our presence. We also know that Mars once had vast oceans of water like those on Earth... *And* that it is absolutely barren of all liquid water and has almost no atmosphere today. Could the same happen to our planet? When we understand why and how the water left Mars, perhaps we can answer this question with some degree of certainty. These are just two obvious issues that highlight the ways in which planetary exploration improves our lives and future. However, these benefits are only secondary in importance. The overwhelming reason to explore the planets is the same as that which exists for all of academia—our pressing drive in the pursuit of knowledge.

We have been capable of exploring the other planets in the solar system for less than 40 years and though we initially started doing so in an aggressive way, the last two decades have shown a dearth of missions leaving the immediate vicinity of our planet. A large part of the reason for this neglect is the tremendous expense associated with planetary exploration. Eventually, space exploration must pay for itself, and this seems to be starting already with the satellite communications industry. However, in the interim, governments fund the effort and it is therefore subject to the whim of public opinion. Expensive projects are the first to suffer in times of shrinking budgets, and for those without obvious and *immediate* benefits like planetary exploration, funding goes away very quickly. Because of this, any research

LIST OF REFERENCES

[Ahuja *et al.* 1993] R. K. Ahuja, T. L. Magnanti, and J. B. Orlin. *Network Flows: Theory, Algorithms. and Applications.* Prentice Hall, Englewood Cliffs, 1993.

[Blamont *et al.* 1986] J. E. Blamont, R. E. Young, A. Seiff, B. Ragent. R. Sagdeev, V. M. Linkin, V. V. Kerzhanovich, A. P. Ingersoll, D. Crisp, L. S. Elson, R. A. Preston, G. S. Golitsyn. and V. N. Ivanov. Implications of the VEGA balloon results for Venus atmospheric dynamics. *Science*, 231:1422–1425, 1986.

[Caddell 1991] T. W. Caddell. Three-dimensional path planning for the NPS II AUV. Master's thesis, US Naval Postgraduate School, December 1991.

[Cormen *et al.* 1990] T. H. Cormen. C. E. Leiserson. and R. L. Rivest. *Introduction to Algorithms.* The MIT Press, Cambridge, 1990.

[Cutts *et al.* 1995] J. A. Cutts, K. T. Nock, J. A. Jones, G. Rodriguez, and J. Balaram. Planetary exploration by robotic aerovehicles. *Journal of Autonomous Robots*, 2(4):261–282, 1995.

[DiCicco *et al.* 1995] A. G. DiCicco, K. T. Nock, and G. E. Powell. Balloon experiment at Venus (BEV). In *JPL Planetary Aerobot Technology Development Program Papers presented at the AIAA 11th Lighter-Than-Air Technology Conference*, Clearwater, May 1995. AIAA, American Institute of Aeronautics and Astronautics.

[Durrant-Whyte and Cox 1990] J. L. H. Durrant-Whyte and I. J. Cox. Dynamic map building for an autonomous mobile robot. In *Proceedings of the IEEE International Workshop on Intelligent Robots and Systems (IROS '90)*, pages 89–96, 1990.

[Eisen 1996] H. J. Eisen. Microrover flight experiment pathfinder mission to Mars. Internet URL http://www-rover.jpl.nasa.gov/projects/rover/mfex.htm, 25 July 1996.

[Gierasch *et al.* 1994] P. J. Gierasch, R. M. Goody, D. Crisp, C. Edwards, A. Del Genio, R. Greeley, A. Hou, R. Kahn, C. B. Leovy, D. McCleese, M. Newman, D. Rider, and R. E. Young. The general circulation of the Venus atmosphere: An assessment. Draft from Astronomy Department, Cornell University, 5 July 1994.

[Golden *et al.* 1987] B. L. Golden, L. Levy, and R. Vohra. The orienteering problem. *Naval Research Logistics*, 34(3):307–318, 1987.

[Golden *et al.* 1988] B. L. Golden, Q. Wang, and L. Liu. A multifaceted heuristic for the orienteering problem. *Naval Research Logistics*, 35(3):359–366, 1988.

[Greeley *et al.* 1994] R. Greeley, G. Schuber, D. Limonadi, K. C. Bender, W. I. Newman, P. E. Thomas, C. M. Weitz, and S. D. Wall. Wind streaks on Venus: Clues to atmospheric circulation. *Science*, 263:358–362, 1994.

65

[Head *et al.* 1996] J. W. Head, III, M. S. Gilmore, G. Collins, L. Crumpler, M. Parry, and R. A. Yingst. Investigation of the application of aerobot technology at Venus: Scientific goals and objectives of the proposed Balloon Experiment at Venus (BEV) and Venus Flyer Robot (VFR). Technical report, Brown University—Department of Geological Sciences, 1 June 1996.

[Heun 1996] M. K. Heun, November 1996. Personal communication while at the NASA Jet Propulsion Laboratory and electronic mail interaction.

[Hou and Goody 1989] A. Y. Hou and R. M. Goody. Further studies of the circulation of the Venus atmosphere. *Journal of the Atmospheric Sciences*, 46(7):991–1001, 1989.

[Hunten *et al.* 1983] D. M. Hunten, L. Colin, T. M. Donahue, and V. I. Moroz, editors. *Venus*. University of Arizona Press, Tuscon, 1983.

[Jones 1995] J. A. Jones. Reversible fluid balloon altitude control concepts. In *JPL Planetary Aerobot Technology Development Program Papers presented at the AIAA 11th Lighter-Than-Air Technology Conference*, Clearwater, May 1995. AIAA, American Institute of Aeronautics and Astronautics.

[Keating 1990] G. M. Keating, editor. *Advances In Space Research*, volume 10 of *The Venus Atmosphere*. The Committee On Space Research (COSPAR), Pergamon Press, New York, 1990.

[Kremnev *et al.* 1986] R. S. Kremnev, V. M. Linkin, A. N. Lipatov, K. M. Pichkadze, A. A. Shurupov, A. V. Terterashvili, R. V. Bakitko, J. E. Blamont, C. Malique, B. Ragent, R. A. Preston, L. S. Elson, and D. Crisp. VEGA balloon system and instrumentation. *Science*, 231:1408–1411, 1986.

[Krogh and Feng 1989] B. H. Krogh and D. Feng. Dynamic generation of subgoals for autonomous mobile robots using local feedback information. *IEEE Transactions on Automatic Control*, 34(5):483–493, 1989.

[Limaye 1990] S. S. Limaye. Venus atmospheric circulation: Known and unknown. In G. M. Keating, editor, *Advances In Space Research*, volume 10 of *The Venus Atmosphere*. The Committee On Space Research (COSPAR), Pergamon Press, New York, 1990.

[Linkin *et al.* 1986a] V. M. Linkin, V. V. Kerzhanovich, A. N. Lipatov, K. M. Pichkadze, A. A. Shurupov, A. V. Terterashvili, A. P. Ingersoll, D. Crisp, A. W. Grossman, R. E. Young, A. Seiff, B. Ragent, J. E. Blamont, L. S. Elson, and R. A. Preston. VEGA balloon dynamics and vertical winds in the Venus middle cloud region. *Science*, 231:1417–1419, 1986.

[Linkin *et al.* 1986b] V. M. Linkin, V. V. Kerzhanovich, A. N. Lipatov, A. A. Shurupov, A. Seiff, B. Ragent, R. E. Young, A. P. Ingersoll, D. Crisp, L. S. Elson, R. A. Preston, and J. E. Blamont. Thermal structure of the Venus atmosphere in the middle cloud layer. *Science*, 231:1420–1422, 1986.

[Lumelsky *et al.* 1990] V. J. Lumelsky, S. Mukhopadhyay, and K. Sun. Dynamic path planning in sensor-based terrain acquisition. *IEEE Transactions on Robotics and Automation*, 6(4):462–472, 1990.

[Moroz 1994] V.I. Moroz. Va-94: Venus atmosphere model for venera-discovery project. White paper, 1994.

[Neto 1994] J. A. R. Neto. A mine search algorithm for the Naval Postgraduate School Autonomous Underwater Vehicle. Master's thesis, US Naval Postgraduate School, December 1994.

[Newman *et al.* 1984] M. Newman, G. Schubert, A. J. Kliore, and I. R. Patel. Zonal winds in the middle atmosphere of Venus from Pioneer Venus radio occultation data. *Journal of the Atmospheric Sciences*, 41(12):1901–1913, 1984.

[Preston *et al.* 1986] R. A. Preston, C. E. Hildebrand, G. H. Purcell, Jr., J. Ellis, C. T. Stelzried, S. G. Finley, R. Z. Sagdeev, V. M. Linkin, V. V. Kerzhanovich, V. I. Altunin, L. R. Kogan, V. I. Kostenko, L. I. Matveenko, S. V. Pogrebenko. I. A. Strukov. E. L. Akim, Yu. N. Alexandrov, N. A. Armand. R. N. Bakitko, A. S. Vyshlov, A. F. Bogomolov, Yu. N. Gorchankov, A. S. Selivanov, N. M. Ivanov, V. F. Tichonov, J. E. Blamont, L. Boloh, G. Laurans, A. Boischot, F. Biraud, A. Ortega-Molina, C. Rosolen, and G. Petit. Determination of Venus winds by ground-based radio tracking of the VEGA balloons. *Science*, 231:1414–1416, 1986.

[Rao 1992] N. S. V. Rao. On performance of path planning algorithms in unknown terrains. *ORSA Journal on Computing*, 4(2):218–224, 1992.

[Rossow 1983] W. B. Rossow. A general circulation model of a Venus-like atmosphere. *Journal of the Atmospheric Sciences*, 40(2):273–301, 1983.

[Sagdeev *et al.* 1986a] R. Z. Sagdeev, V. M. Linkin, J. E. Blamont, and R. A. Preston. The VEGA Venus balloon experiment. *Science*, 231:1407–1408, 1986.

[Sagdeev *et al.* 1986b] R. Z. Sagdeev, V. M. Linkin, V. V. Kerzhanovich, A. N. Lipatov, A. A. Shurupov, J. E. Blamont, D. Crisp, A. P. Ingersoll, L. S. Elson, R. A. Preston, C. E. Hildebrand, B. Ragent, A. Seiff, R. E. Young, G. Petit, L. Boloh, Yu. N. Alexandrov, N. A. Armand, R. V. Bakitko, and A. S. Selivanov. Overview of VEGA Venus balloon in situ meteorological measurements. *Science*, 231:1411–1414, 1986.

[Schwartz and Sharir 1988] J. T. Schwartz and M. Sharir. A survey of motion planning and related geometric algorithms. *Artificial Intelligence*, 37(1):157–169, 1988.

[Sposato 1995] J. J. Sposato. Optimal routing of ice reconnaissance aircraft. Master's thesis, US Naval Postgraduate School, September 1995.

[Tsiligirides 1984] T. Tsiligirides. Heuristic methods applied to orienteering. *Journal of the Operational Research Society*, 35(9):797–809, 1984.

[Twicken 1996] J. Twicken. Sample temperature and pressure profiles. Internet URL `http://www-star.stanford.edu/projects/mgs/profile.html`, 26 August 1996.

[White 1958] T. H. White. *The Once and Future King.* Collins, London, 1958.

[Wren and Holliday 1972] A. Wren and A. Holliday. Computer scheduling of vehicles from one or more depots to a number of delivery points. *Operational Research Quarterly*, 23(3):333–344, 1972.

INITIAL DISTRIBUTION LIST